Hingepoints and neural folds reveal conserved features of primary neurulation in the zebrafish forebrain

Jonathan M. Werner[1*], Maraki Y. Negesse[1*], Dominique L. Brooks[1], Allyson R. Caldwell[1], Jafira M. Johnson[1] and Rachel M. Brewster[1]

1. Department of Biological Sciences, University of Maryland Baltimore County, Baltimore, MD 21250

* These authors contributed equally to the manuscript

ABSTRACT

Primary neurulation is the process by which the neural tube, the central nervous system precursor, is formed from the neural plate. Incomplete neural tube closure occurs frequently, yet underlying causes remain poorly understood. Developmental studies in amniotes and amphibians have identified hingepoint and neural fold formation as key morphogenetic events and hallmarks of primary neurulation, the disruption of which causes neural tube defects. In contrast, the mode of neurulation in teleosts such as zebrafish has remained highly debated. Teleosts are thought to have evolved a unique pattern of neurulation, whereby the neural plate infolds in absence of hingepoints and neural folds (NFs), at least in the hindbrain/trunk where it has been studied. We report here on zebrafish forebrain morphogenesis where we identify these morphological landmarks. Our findings reveal a deeper level of conservation of neurulation than previously recognized and establish the zebrafish as a model to understand human neural tube development.

INTRODUCTION

Primary neurulation is the process by which the neural tube, the precursor of the brain and spinal cord, is shaped from the neural plate. These morphogenetic events have mostly been studied in amniotes (mouse and chick) and amphibians (frogs), where conserved mechanisms were identified. Following neural induction, the neural plate (Supplemental Figure S1A) narrows and elongates by convergent extension movements[1,2]. The morphology of the neural plate is further changed in a biphasic manner[3]. The first morphological event is the formation of the medial hingepoint (MHP), which bends the flat neural plate into a V shape, forming the neural groove (Supplemental Figure S1B). Neural Folds (NFs) at the edges of the neural plate subsequently elevate, a process that is further driven by head mesenchyme expansion[4]. In the second phase, the neural plate folds at paired dorso-lateral hingepoints (DLHPs), bringing the NFs closer together (Supplemental Figure S1C). The NFs eventually meet and fuse at the midline, completing neural tube formation. The dorsal midline is subsequently remodeled to separate the inner neuroectoderm from the outer non-neural ectoderm fated to become the epidermis (Supplemental Figure S1D). In the cranial region of amniotes, neural tube closure is initiated at several sites and extends via a zippering process from these closure points to seal the neural tube. Incomplete cranial neural tube closure occurs frequently, resulting in anencephaly and exencephaly[3].

Several cellular mechanisms have been identified that contribute to the bending of the neural plate, among which apical constriction is the most studied[5–8]. A meshwork of F-actin accumulates at the apical cortex of neuroectodermal cells and contracts, thereby reducing the cell apex (Supplemental Figure S1b1). The contraction is driven by myosin that co-localizes with F-actin at the apical pole. Disruption of F-actin using drug inhibitors or genetic

60 tools causes severe cranial neural tube defects[5,9–14]. Similarly, treatment with blebbistatin, an
61 inhibitor of non-muscle myosin II activity, impairs apical constriction in the superficial layer of
62 the *Xenopus* neural plate[15].

63 In contrast to hingepoint formation, the cell intrinsic mechanisms that shape NF cells
64 are less understood. The NFs are bilaminar, consisting of a layer of neuroectoderm capped
65 by a layer of non-neural ectoderm[16], a topology that is acquired via epithelial ridging, kinking,
66 delamination and apposition[16,17]. NF fusion involves the formation of cellular protrusions that
67 span the midline gap and establish the first contact and attachment points with NF cells from
68 the contralateral side[18–20] (Supplemental Figure S1c1). There is little consensus on the cell
69 type (neuroectoderm or non-neural ectoderm) that generates the cellular protrusions as it
70 varies depending on the species and the axial level. In the mouse forebrain, the initial contact
71 is made by neuroectodermal cells[18,21–24]. Disruption of F-actin blocks the formation of
72 protrusions and prevents NF fusion[20], revealing the central role of these cellular processes.

73 While more anterior regions of the neural tube undergo primary neurulation as
74 described above, most vertebrates also exhibit a distinct type of neural tube formation in
75 more posterior regions, termed secondary neurulation. During this process, a mesenchymal
76 cell population condenses into a solid neural rod that subsequently epithelializes and forms a
77 central lumen[25,26]. In zebrafish, the neural tube in the hindbrain and trunk region initially forms
78 a solid rod that later develops a lumen, a process seemingly analogous to secondary
79 neurulation[27]. However, examination of the tissue architecture in zebrafish[28–30] and other
80 teleosts[31,32] revealed that the neural rod is shaped by infolding of a neural plate (albeit
81 incompletely epithelialized), which best fits the description of primary neurulation[33]. Despite
82 this evidence, differences in tissue architecture, the multi-layered architecture of the neural

83 plate and the apparent lack of hingepoints, neural groove and NFs are difficult to reconcile
84 with a mode of primary neurulation and have contributed to the persistent view that neural
85 tube formation in teleosts is different than in other vertebrates[34–36].

86 We show here that, in contrast to the zebrafish hindbrain and trunk region, the process
87 of neural tube formation in the forebrain exhibits many of the hallmarks of primary
88 neurulation. We observe the presence of hingepoints and NFs in the epithelialized anterior
89 neural plate (ANP), demonstrate that formation of the MHP involves oscillatory apical
90 contractions that progressively reduce the apical surface, and show that disruption of myosin
91 function impairs apical constriction of these cells and NF convergence. We further show that
92 neural tube closure is initiated at two separate sites in the forebrain and that fusion of the NFs
93 is mediated by filopodial-like extensions of neuroectodermal cells that bridge the midline.
94 These findings identify conserved mechanisms of primary neurulation that were previously
95 overlooked in teleosts and support the suitability of zebrafish for understanding the etiology of
96 human neural tube defects.

RESULTS

Precocious epithelialization of the anterior neural plate is associated with bending

The zebrafish ANP is quite distinct from the neural plate in more posterior regions, as it undergoes precocious epithelialization[37]. To assess whether epithelialization correlates with a change in the mode of neurulation, we examined the morphology of the neuroectoderm in optical cross sections at developmental stages ranging from 2 to 10 somites (som). We observed that at 2-5 som the ANP has a V shape marked by a medial neural groove (black arrowhead) flanked by the elevated lateral edges of the ANP (white arrowhead), which are reminiscent of NFs (Figure 1A-B). By 7 som the groove is no longer visible and the elevated edges of the ANP have fused medially (Figure 1C, white arrowhead) and form a dorsal bulge (Figure 1C-D, white arrowhead). These observations suggest that the ANP bends at the midline, which correlates with elevation of the lateral edges of the ANP.

The anterior neural plate is multi-layered and gives rise to the eyes and forebrain

The central part of the ANP is fated to become the eyes, while its lateral edges produce the dorsally-located telencephalon and the ventral-most ANP region gives rise to the hypothalamus/ventral diencephalon[37,38]. To gain a better understanding of the morphogenetic events that shape the ANP, we examined transverse views of transgenic Tg[*emx3:YFP*] embryos at developmental stages 2, 5, 7 and 10 som, in which telencephalon precursors are labeled[39]. We observed, as previously described[37], that the ANP is a multi-layered tissue, with a mesenchymal superficial core and a marginal or deep layer. These layers will henceforth be referred to as the superficial and deep layers, respectively (s and d in Figure 1E-F). The YFP-positive lateral edges of the ANP elevate, migrate over the eye field and fuse

120 medially at 7 som to form the telencephalon (Figure 1G-H). By 7 som the multilayered ANP
121 resolves into a single-cell layered neuroectoderm (Figure 1G). While the morphological
122 changes and cellular dynamics that form the eyes are quite well understood[37,38], the
123 accompanying events that shape the forebrain are for the most part unknown and the focus
124 of the current study.
125
126 **Presence of hingepoints and neural folds in the anterior neural plate**
127 To investigate whether the ANP bends and folds around hingepoints to bring NFs in close
128 apposition, we examined the cytoarchitecture of this tissue in embryos at stages 2-10 som,
129 labeled with phalloidin (filamentous (F) actin), anti-Sox3 (neural cells) and anti-p63
130 (epidermal cells, nuclear label) (Figure 1I-L).
131 We found that at 2 som, neural cells appear mesenchymal with no visible polarized
132 enrichment of F-actin (Figure 1I), consistent with previous observations[37]. The epidermis at
133 this stage is in a far lateral position (white arrowhead in Figure 1I).
134 Between 2 and 5 som, clusters of cells in the superficial and deep layers of the eye
135 field have been reported to undergo early epithelialization[37], which we confirm here with foci
136 of F-actin enrichment in the medial/superficial region (M in Figure 1J, M) and in two dorso-
137 lateral clusters in the deep marginal layer (DL in Figure 1J, M). The apical surfaces of the
138 superficial cells appear to constrict and orient towards the midline, resulting in the formation
139 of a medial neural groove (asterisk in Figure 1M). Similarly, the paired dorso-lateral clusters
140 of cells in the deep layer are also apically constricted and the neuroectoderm folds sharply at
141 this level (red arrows in Figure 1M). These data suggest that the medial and dorso-lateral
142 cells enriched for apical F-actin may function as hingepoints. Similarly to amphibians whose

143 neural plate is bilayered[40], the putative medial hingepoint in the zebrafish ANP forms in the
144 superficial layer and is therefore more dorsally positioned than its chick and mouse
145 counterpart. However, these cells eventually sink inwards, as revealed by fate mapping using
146 photoconvertible membrane-targeted Kaede (mKaede) to label this cell population
147 (Supplemental Movie 1). These findings are consistent with a previous study showing that
148 superficial cells radially intercalate between deep marginal cells[37], which contributes to the
149 expansion of the optic vesicles (Figure 1G-H). Zebrafish dorso-lateral hingepoints do not
150 undergo these cellular rearrangements as they form in the deep layer.

151 The lateral edges of the ANP are bilaminar at 5 som, consisting of a layer of
152 neuroectoderm cells capped by a layer of p63-positive non-neural ectoderm (and Sox3/p63-
153 negative olfactory placodal cells bridging the two layers), indicative of a NF structure (Figure
154 1J, M). The YFP-positive ANP cells in Tg[*emx3:YFP]* embryos correspond to the
155 neuroectoderm component of the NF (Figure 1F), revealing that the tip of the NF gives rise to
156 the telencephalon. At 4 som, the YFP-positive region of Tg[*emx3:YFP*] embryos extends the
157 length of the forebrain (Figure 1O), delineating the anterior-posterior range of the NFs.

158 The NF and putative hingepoints are transient as they are no longer observed in 7
159 som embryos. By this stage, the tips of the NFs have converged medially and fused, forming
160 the telencephalon (Figure 1K). These cells are enriched in apical F-actin at 10 som,
161 suggesting that they epithelialize (Figure 1L). The non-neural ectoderm still occupies a lateral
162 position at 7 som (Figure 1K, arrowheads), however by 10 som these cells migrate and fuse
163 dorsally (single arrowhead in Figure 1L), indicating that, as observed in mice, the
164 neuroectodermal component of the NFs meet first (Supplemental Figure S1)[21,22].
165 Measurements of the distance between the medial-most p63-positive domain and the dorsal

166 midline at stages 2-7 som indicate that the non-neural ectoderm portion of the NFs converges
167 steadily towards the midline and may provide a lateral force that contributes to the
168 displacement of NFs (Figure 1N).
169 These observations reveal that transient medial and dorso-lateral epithelialized cell
170 clusters may be the functional equivalents of the MHP and paired DLHPs of amniotes (and
171 will be referred to henceforth as such), as they form at the right time and place to contribute
172 to the formation of the neural groove (MHP), bending of the neuroectoderm and medial
173 convergence of the NFs.
174
175 **Cell shape changes underlying dorso-lateral hingepoint and neural fold formation**
176 To capture the dynamics of NF formation and image cells at higher resolution, we mosaically
177 expressed membrane-targeted GFP (mGFP) and imaged embryos at the 2-10 som stages in
178 transverse sections (Figure 2). 3D reconstructions of some of these images were generated
179 to visualize the spatial relation between labeled cells (Supplemental Movie 2, 3).
180 At 2 som, cells in the deep layer have a columnar shape with one end in contact with
181 the basal lamina and a future apical surface oriented towards the midline (Figure 2A). These
182 cells extend membrane protrusions into the superficial layer, which may promote radial
183 intercalation (inset in Figure 2A).
184 At 5 som, cells in the dorso-lateral deep layer have undergone apical constriction and
185 basal expansion, forming DLHPs (yellow dotted circles and double arrowheads in Figure
186 2B,b1; Supplemental Movie 2). These cell shape changes may initiate the outpocketing of the
187 optic vesicles (ov in Figure 2B,b1). The bilaminar organization of the NFs is clearly visible at
188 this stage. Neuroectodermal cells within the NFs (arrows in Figure 2b1 and c1) are elongated

189 and their basal poles are constricted, giving them the appearance of fanning out from a focal
190 point (red circles in Figure 2b1 and c1). Furthermore, their plasma membrane is ruffled,
191 indicative of protrusive activity (Supplemental Movie 2).

192 By 7 som (Figure 2D, Supplemental Movie 3), neuroectodermal cells of the NFs have
193 reached the dorsal midline. They maintain their organization with basal poles constricted and
194 clustered at a focal point on the basement membrane (red circle in Figure 2d1). 3D
195 reconstructions reveal that these cells are finger-shaped as they extend across the dorsal
196 midline. DLHP cells maintain their apical constriction/basal expansion and further elongate,
197 contributing to the expansion of the optic vesicles (dotted double arrowhead in Figure 2d1).

198 At 10 som (Figure 2E, e1) deep cells in the eye field and NFs have a columnar,
199 epithelial organization. Consistent with previous findings, eye field cells shorten along their
200 apico-basal axis by contracting their apical processes and coincidently transition to a more
201 dorso-ventral orientation[37] (dotted double arrow in Figure 2e1). Cuboidal non-neural
202 ectoderm cells cover the dorsal surface of the newly formed telencephalon (arrowheads in
203 Figure 2e1.

204 The dynamic cell shape changes in the deep layer of the neuroectoderm were
205 quantified by measuring cell length and the apico:basal ratio of mGFP-labeled cells located at
206 different positions along the medio-lateral axis of the ANP at 2, 5 and 7 som (Figure 3).
207 These data reveal that the average length of DLHP cells increases while their apical:basal
208 ratio decreases between 2 and 7 som, coincident with optic vesicle evagination. They also
209 confirm that neuroectodermal cells of the NFs adopt the opposite configuration (reverse
210 hingepoints), with basally constricted poles.

211 To capture the dynamics of NF formation, we performed transverse view time-lapse
212 imaging of WT embryos expressing mKaede or Tg[*emx3:YFP*] transgenic embryos
213 expressing membrane-targeted RFP (mRFP) (n=2 embryos, Figure 4; Supplemental Movies
214 1 and 4. We observed that as the NFs elevate (blue dotted line in Figure 4A-C), NF cells
215 basally constrict (red outline and arrow in Figure 4a1-c1). Interestingly, this cell behavior
216 appears restricted to cells within the *emx3* expression domain (Figure 4D-f1).
217 These findings indicate that zebrafish DLHP cells adopt a wedge shape similar to their
218 counterparts in amphibians and amniotes, which enables epithelial folding. They further
219 identify basal constriction of NF cells as a cell shape change that contributes to NF formation.
220

221 **Medial hingepoint cells constrict apically and elongate**

222 While mosaic expression of mGFP enabled high resolution imaging of DLHPs and NFs, it
223 resulted in fewer cells labeled in the medial superficial layer, where the MHP forms.
224 Phalloidin labeling was therefore used to image these cells in 2 and 5 som embryos.
225 At the 2 som stage, some medial/superficial cells immediately below the enveloping
226 layer (EVL) are apically constricted, forming the MHP (Figure 5A-a2). By 5 som, MHP cells
227 appear more densely packed, the majority of them are apically constricted and oriented
228 towards the midline. Concomitant with these cell shape changes and the medial convergence
229 of NFs, MHP cells shift to a more ventral position (Figure 5B-b2). A small opening, the neural
230 groove, is observed immediately above the MHP at this stage (NG in Figure 5b1).
231 Measurements of the apico:basal surface ratio of MHP cells in 5 som embryos
232 confirmed that they are wedge-shaped (Figure 5c1). Similar to amphibians[41], apical
233 constriction appears tightly coupled to cell elongation, as the length-to-width ratio (LWR) of

234 MHP cells increases significantly between 2 and 5 som (Figure 5c2). Thus, both apical
235 constriction and cell elongation appear to shape the MHP and contribute to tissue-level
236 morphogenesis.

237 Another contributing factor to hingepoint formation in amniotes is the basal location of
238 nuclei in both the medial and lateral hingepoints[42,43]. However, in zebrafish embryos, the
239 relative position of the nucleus in medial superficial cells at 2 and 5 som does not change
240 significantly and is therefore unlikely to contribute to wedging of these cells.

241

242 **Oscillatory constrictions reduce the apical surface of medial hingepoint cells**

243 To gain a better understanding of the dynamics of apical constriction and cell internalization,
244 the ANP of embryos ubiquitously expressing mGFP was imaged from a dorsal view using
245 time-lapse microscopy between 2 som to 4 som (n = 2 embryos, Figure 5D and Supplemental
246 Movie 5). The focal plane was set immediately below the EVL, at the level of the MHP. These
247 movies revealed clusters of medially-located cells that undergo progressive cell surface
248 reduction (color-coded in Figure 5d1-d7), while the surface area of adjacent, more lateral
249 cells remained unchanged for the duration of imaging (yellow asterisks in Figure 5d1-d6).
250 EVL cells came into focus immediately posterior to the cells with reducing apices. Since the
251 EVL is drawn inward as a result of its close contact with apically constricting MHP cells
252 (Figure 5B-b2), we surmise that apical constriction proceeds in a posterior-to-anterior
253 direction. In later movie frames, EVL cells are no longer observed within the field of view,
254 coinciding with the proximity of the NFs to the midline (Supplemental Movie 5). This indicates
255 that medial EVL cells eventually lose contact with the MHP and return to their original
256 position, allowing the NFs to fuse at the dorsal midline (Figure 1J-K).

257 To further examine the dynamics of apical constriction, the surface area of superficial
258 ANP cells was measured at shorter intervals. Midline cells presumed to be part of the MHP
259 (20 μm on either side of the midline, Figure 6A, E) or cells immediately adjacent to the MHP
260 (greater than 20 μm on either side of the midline, Figure 6B) were scored. This analysis
261 revealed that individual cells in both populations undergo oscillatory constrictions. Between
262 constrictions, the surface areas of cells re-expand with gradually decreasing amplitude
263 (Figure 6A, E), which is most pronounced in MHP cells. The time of oscillation between two
264 expanded states revealed no significant difference between both groups (Figure 6C, median
265 oscillation time of 45 seconds). Likewise, there was no significant difference in the timing of
266 individual constrictions. However, it appears that MHP cells spent less time expanding than
267 MHP-adjacent cells (15 seconds median time for MHP vs 30 second for MHP-adjacent,
268 Figure 6D).
269 Together these data indicate that MHP cells and their neighbors undergo progressive
270 narrowing of their apical pole via oscillatory constrictions and that these cellular dynamics
271 proceed in a posterior-to-anterior direction.
272
273 **Neural fold fusion is initiated at closure points and mediated by protrusive activity**
274 In mice, neurulation proceeds unevenly along the anterior-posterior axis with multiple closure
275 initiation sites[3], raising the question of whether NF fusion also occurs asynchronously in
276 zebrafish. To address this, we performed time-lapse imaging of embryos mosaically
277 expressing mGFP from a dorsal view around the time when opposing NFs approach the
278 midline (n= 2 embryos, Figure 7A and Supplemental Movie 6). Neuroectodermal cells of the
279 NF were identified based on their elongated shape and dorsal location.

280 These movies revealed that the NFs have an arc shape with the apex positioned
281 anteriorly (red asterisks in Figure 7A), similar to the expression domain of the telencephalon
282 marker *emx3* at the onset of NF convergence (inset in Figure 7A). NF fusion is initiated near
283 the apex of the arch and proceeds in an anterior-to-posterior direction for a distance of
284 approximately 35 μm (red dotted line in Figure 7a3). At this level, defined as closure point
285 one (C1 in Figure 7a3), NF fusion proceeds asynchronously as a second closure initiation
286 site is formed more posteriorly (C2 in Figure 7A5). These closure points define an eye-
287 shaped opening (white dotted oval in Figure 7a4, a5) and a zippering process begins at the
288 anterior and posterior corners of this structure, progressing from both ends toward the middle
289 (Figure 7a6,a7; Supplemental Movie 6).
290 The events that complete NF fusion in amniotes involve the extension of dynamic
291 cellular projections towards the midline[18–20]. Likewise, we observed that zebrafish
292 neuroectodermal cells extend filopodia to establish contact with cells from the contralateral
293 side. Furthermore, the cell bodies appear to hyper-extend beyond the midline (Figure 7b3, b4
294 and Supplemental Movie 7), suggesting that they interdigitate between cells of the opposing
295 NF. These cellular extensions are eventually retracted, as the midline becomes well defined
296 after epithelialization (Figure 1L).
297 The presence of closure points and the usage of filopodia to establish contact with NF
298 cells across the midline reveal additional aspects of forebrain neurulation that are conserved
299 in zebrafish.
300
301 **Temporal overlap in the timing of key cell shape changes in the anterior neural plate**

302 In amniotes, MHP formation precedes the shaping of paired DLHPs and initiates NF
303 elevation. To reveal the relative timing of cell shape changes in zebrafish and their
304 contributions to ANP morphogenesis, we plotted tissue dynamics using measurements from
305 transverse time-lapse movies (n= 2 embryos, data shown for 1 embryo, Supplemental Movie
306 1). We observed that changes in the neural groove angle (indirect measurement of MHP
307 apical constriction), the optic vesicle angle (which reflects DLHP apical constriction) and the
308 basal NF angle (a proxy for basal constriction) occur concurrently and temporally correlate
309 with NF elevation and convergence (Figure 8). This analysis revealed that, in contrast to
310 amniotes, key cell shape changes in the ANP do not occur in a clear chronological manner
311 and that one or more of these events are likely to contribute to ANP morphogenesis.
312

313 **Molecular characteristics of medial and lateral hingepoints**

314 Key features of cells that form hingepoints include apico-basal polarization as well as an
315 accumulation of an apical contractile machinery composed of actin filaments (F-actin) and
316 non-muscle myosin II[44]. To test whether the MHP and DLHPs in the zebrafish forebrain have
317 some or all of these characteristics, the localization of apical markers Pard3-GFP (transiently
318 expressed following mRNA injection), ZO-1 (anti-ZO-1) and N-cadherin (anti-N-cad) was
319 examined along with F-actin (phalloidin) and phospho-Myosin Light Chain II (anti-P-MLC) in 5
320 som embryos (Figure 9).

321 Apical co-localization of F-actin with Pard3-GFP (Figure 9A-c2), ZO-1 (Figure 9D-f2),
322 and N-cad (Figure 9G-i2) was confirmed in both the MHP and DLHPs at 5 som. Thus, while
323 the establishment of apico-basal polarity is generally delayed in the zebrafish neural plate
324 relative to amniotes, the cell clusters that undergo apical constriction in the ANP epithelialize

325 precociously. P-MLC accumulation at the apical pole is also apparent by the 5 som stage in
326 MHP cells where it overlaps with F-actin (Figure 9J-l2). In contrast, P-MLC apical enrichment
327 is not observed in the DLHPs (arrowhead in Figure 9K,l2). P-MLC does however accumulate
328 in the cell cortex of all neuroectodermal cells where it overlaps with F-actin, in addition to the
329 basal surface of EVL cells (arrow in Figure 9K, l1) and at the interface between the
330 neuroectoderm and non-neural ectoderm (dotted line in Figure 9K-L).
331 These findings confirm that both the MHP and DLHP undergo early epithelialization
332 and accumulate apical markers. However, the MHP and DLHPs are molecularly distinct
333 structures given that the latter is not enriched for P-MLC.
334
335 **Myosin contractility is required for medial hingepoint formation and neural fold**
336 **convergence**
337 During neural tube closure, the actomyosin cytoskeleton is thought to be a driving force for
338 apical constriction[41]. To address whether this molecular motor mediates apical constriction in
339 zebrafish, non-muscle myosin II (NMII) was blocked using blebbistatin and a translation-
340 blocking morpholino (MO) targeting NMIIb[45] and the effect was analyzed in 5 som embryos
341 that were labeled to reveal the localization of F-actin (phalloidin) and P-MLC (anti-P-MLC).
342 Both treatments resulted in the absence of a clearly defined MHP (Figure 10a1,a1' vs 10b1,
343 b1', c1 and c1'). LWR scores for these cells were close to 1 (Figure 10D), indicative of cell
344 rounding, which prevented measurement of their apical:basal surface ratio. In contrast, while
345 the length of DLHPs in treated embryos was reduced (Figure 10D), these cells retained their
346 wedge shape (Figure 10a2,a2' vs b2, b2', c2, c2), with apical:basal surface ratios of less than
347 1 (Figure 10E). These observations are consistent with the lack of apical P-MLC enrichment

348 in DLHP cells and support a conserved function for actomyosin in driving apical constriction
349 of MHP cells.

350 At a morphological level, disruption of the actomyosin network causes neural tube
351 defects that trace back to impaired apical constriction and convergent extension in *Xenopus*
352 embryos[15]. To test whether myosin is similarly required for forebrain neural tube closure in
353 zebrafish, control (untreated and DMSO-treated) and blebbistatin-treated embryos were
354 labeled at the 2, 5 and 7 som stage via *in situ* hybridization using the telencephalon marker
355 *emx3* (Figure 10F) and the width of the posterior-most *emx3* domain was measured (Figure
356 10G). In contrast to control embryos, NF convergence was impaired in blebbistatin-treated
357 embryos, beginning at the 5 som stage. It is possible that earlier convergent extension
358 defects in the ANP contribute to this phenotype. However, failure of MHP cells to undergo
359 apical constriction is likely to be a contributing cause given that disruption of several other
360 proteins implicated in this process, including Shroom3[13] and GEF-H1, a RhoA-specific GEF[14]
361 results in severe neural tube closure defects.

362

363 **DISCUSSION**

364 We report here on mechanisms of forebrain morphogenesis in the zebrafish embryo and
365 reveal that this region of the brain is formed by primary neurulation, involving the use of
366 hingepoints and NFs.

367 The zebrafish MHP and paired DLHPs form in the superficial and deep layers of the
368 eye field, respectively. The timing of MHP and DLHP formation overlap in zebrafish, in
369 contrast to the biphasic nature of these events in mouse[3]. The zebrafish MHP is cup-shaped
370 and more transient than its mammalian counterpart since these cells eventually intercalate

371 between deep layer cells, contributing to the expansion of the eye vesicle[37]. Hingepoints are
372 restricted to the ANP in zebrafish, however they are also present in more posterior regions in
373 amniotes. Despite this difference, individual cells in the medial zone of the hindbrain neural
374 plate were recently shown to internalize via a myosin-dependent mechanism[46]. Such
375 variation from the organized cell clusters forming hingepoints in the zebrafish forebrain could
376 be explained by precocious epithelialization of the ANP[37]. It thus appears that there is a
377 transition from clustered internalization in the forebrain to individual cell internalization in the
378 hindbrain region.

379 A key feature of hingepoint cells is their reduced apical surface, which is in part due to
380 actomyosin contractility[13,41,47,48]. Apical constriction is thought to function as a purse string to
381 generate the force required to bring the NFs together during cranial neurulation[49]. We provide
382 evidence that the zebrafish MHP also utilizes an actomyosin-based contractile system.
383 Assembly of this actomyosin network occurs via oscillatory constrictions with gradually
384 decreasing amplitude, akin to the ratchet model initially proposed in invertebrates[50–52] and
385 later reported during neural tube closure in *Xenopus*[53]. We further show that disruption of
386 myosin impairs NF convergence, possibly by contributing a “pulling force” on the NFs or by
387 clearing the dorsal midline of eye field cells. These observations suggest that the actomyosin
388 machinery is used across vertebrate to drive cranial neural tube closure and it will be
389 interesting in the future to test whether upstream regulators of apical constriction such as
390 Shroom3[13] are also conserved.

391 In contrast to the MHP, the paired DLHPs do not require myosin to apically constrict,
392 suggesting that DLHP formation is regulated by a distinct mechanism. Consistent with this
393 observation, cell packing at a dorso-ventral boundary in the mouse neural tube causes

394 buckling of the neuroectoderm at the DLHPs[54]. It is possible that such a mechanism also
395 operates during zebrafish neurulation. Actomyosin may however generate cortical tension[15],
396 enabling both MHP and DLHP cells to maintain their elongated shape.

397 NFs in chick embryos form via epithelial ridging, kinking, delamination and
398 apposition[16], although the cellular basis of these morphogenetic events is not well
399 understood. Elevation of the NFs in the mouse cranial neural plate is dependent on MHP
400 constriction and expansion of the head mesenchyme[55]. NFs in the zebrafish are restricted to
401 the ANP and head mesenchyme is unlikely to play a significant mechanical role in NF
402 elevation, as the mesoderm layer underlying the ANP is thin. We instead identify basal
403 constriction as a NF-intrinsic cell behavior that functions as a “reverse hingepoint”. Basal
404 constriction may contribute to the early stages of NF elevation or ridging/kinking (implicated in
405 the acquisition of the bilaminar topology of the NFs). Based on scanning EM images of chick
406 embryos, it appears that this cell behavior may also be conserved in amniotes[16,17].

407 The final step of primary neurulation involves the convergence and fusion of the NFs
408 at the dorsal midline. NF convergence in zebrafish is likely to be mediated by cell intrinsic
409 forces, including MHP and DLHP formation, although it is difficult to parse out their relative
410 contribution, in addition to extrinsic forces derived from the non-neural ectoderm[17]. NF fusion
411 is initiated at closure points in mammals and birds[56]. We observe two closure points in the
412 zebrafish forebrain that form an eye-shaped opening that narrows from the corners in a
413 bidirectional manner. Fusion of the NFs is mediated by the formation of cell protrusions that
414 span the midline and establish the first points of contact with NF cells from the contralateral
415 side. Akin to mice[21,22], the cells that initiate contact between apposing NFs in zebrafish derive
416 from the neuroectodermal portion of the NFs. However, rather than establishing contact and

417 adhering via their lateral surfaces, the protrusive ends of zebrafish neuroectoderm cells
418 appear to transiently interdigitate between their contralateral counterparts, forming a rod-like
419 structure, the precursor of the telencephalon. These hyperextensions are later retracted as
420 the telencephalon eventually epithelializes, forming a clearly defined midline. Once the
421 neuroectoderm cells have met and fused, non-neural ectoderm cells complete their migration
422 and fuse at the dorsal midline, forming a continuous epidermal layer.

423 In addition to the epidermis, frog and fish embryos are surrounded by an outer
424 protective epithelial monolayer, called EVL in zebrafish. Given that the EVL is in direct
425 contact with the NFs, it is possible that this epithelial layer contributes to forebrain
426 morphogenesis by providing a stable substrate for NF convergence. Conversely, the EVL is
427 transiently tugged inward as the MHP cells undergo apical constriction. It is therefore likely
428 that the interactions between the neural ectoderm and the EVL are reciprocal.

429 Taken together, these findings reveal striking similarities and some unique features of
430 forebrain neurulation in fish that have significant implications for our understanding of the
431 evolution of neurulation and the relevance of zebrafish to understand human neural tube
432 development.

433

434 **METHODS**

435 **Zebrafish strains/husbandry**

436 Studies were performed using wildtype (AB) strains or *Tg(emx3:YFP)*^{b1200} [39] and embryos
437 were raised at 28.5°C. All experiments were approved by the University of Maryland,
438 Baltimore County's Institutional Animal Care and Use Committee (IACUC) and were
439 performed according to national regulatory standards.

440

441 **Nucleic acid and morpholino injections**

442 Plasmids encoding membrane-targeted Green Fluorescent Protein (mGFP) (Richard
443 Harland, University of California, Berkeley, CA, USA), membrane-targeted Red Fluorescent
444 Protein (mRFP), membrane-targeted Kaede (mKaede) (a gift from Ajay Chtinis, National
445 Institute of Health, Bethesda, MD) and *pard3:egfp*[57] were linearized with NotI and transcribed
446 using the SP6 mMESSAGE mMACHINE kit (Ambion, AM1340). For ubiquitous expression of
447 *mGF*P, *mRFP*, *mkaede* or *par3d:eGFP*, 50 pg of RNA was injected into 1-cell stage embryos.
448 For mosaic expression of mGFP, 50 pg of RNA was injected into 1 or 2 of the four central
449 blastomeres at the 16-cell stage. These blastomeres have a high probability for neural fate[58]
450 and are easy to identify for reproducible injections.
451 MOs were designed and synthesized by GeneTools (Philomath, Oregon, USA) and injected
452 into 1-cell stage embryos. *mhy10*(Non-muscle Myosin IIB, EXON2-intron2) was delivered at
453 3ng per injection.
454 *mhy10*: 5'-CTTCACAAATGTGGTCTTACCTTGA-3′ [45]
455
456 Microinjections were performed using a PCI-100 microinjector (Harvard Apparatus, Holliston,
457 MA, USA).

458

459 **Blebbistatin treatment**

460 90% epiboly embryos were manually dechorionated in an agarose-covered petri dish with E3
461 medium. Once embryos reached the tailbud stage, they were placed into 50μM blebbistatin
462 (B0560 Sigma-Aldrich) diluted with E3 and then incubated at 28.5^{o}C. Stock solution of
463 blebbistatin was prepared with DMSO as per manufacturer's instructions. Accordingly, a
464 control group of embryos were treated with 1% DMSO diluted with E3 alongside every
465 blebbistatin trial. Once the desired developmental stage was reached (2-, 5-, or 7-som),
466 embryos were immediately fixed with 4% paraformaldehyde (PFA). As blebbistatin is light
467 sensitive, embryos were kept in the dark as much as possible until fixation.

468

469 **Fixed tissue preparations and immunolabeling**

470 Embryos were fixed in 4% PFA for 16 hours at 4°C overnight. Immunolabeling was performed
471 on whole mount embryos, which were then sectioned with a Vibratome (Vibratome 1500
472 sectioning system), with the exception of N-cadherin, which was done on sections. Primary
473 antibody incubation was performed for 24-48 hours at 4°C and secondary antibody incubation
474 for 2.5 hours at room temperature.

475 Antibodies used: Rabbit anti-GFP at 1:1000 (Invitrogen, A11122), Rabbit anti-Sox3c at
476 1:2000 (Gift from Michael Klymkowsky), Rabbit anti-P-myosin light chain at 1:50 (Cell
477 Signaling Technology, #3671S), Mouse anti-p63 at 1:200 (Santa Cruz BioTechnology, SC-
478 8431 no longer in production), Rabbit anti-N-cadherin at 1:50 (Abcam, ab211116) and Mouse
479 anti-ZO-1 antibody at 1:100 (Invitrogen, 33-9100). Alexa Fluorophore secondary antibodies
480 were all used at a 1:1000 concentration: Goat anti-Rabbit -488, -568, -594 and Goat anti-
481 Mouse -488, -594.Alexa Fluor 488-conjugated or 594-conjugated Phalloidin (Invitrogen,

482 A12379 and A12381) at 1:250 and DAPI (Invitrogen, D1306) were used according to
483 manufacturer's instructions. Sections were mounted on glass slides using ProLong Diamond
484 Antifade Mountant (Invitrogen, P36961). *Tg(emx3:YFP)*^{b1200} embryos were immunolabeled
485 with anti-GFP to amplify the signal. mGFP and *pard3:eGFP*-injected embryos were not
486 immunolabeled with anti-GFP.
487

488 **Whole-mount *in situ* hybridization and imaging**

489 *In situ* hybridization was performed as described[59]. *emx3* riboprobe template was generated
490 by PCR amplification using cDNA from 24hpf embryos.

491 T7 promoter: **TAATACGACTCACTATAGGG**
492
493 *emx3* antisense:
494 FWD: TCCATCCATCCTTCCCCCTT
495 RVS: **TAATACGACTCACTATAGGG**GTGCTGACTGCCTTTCCTCT
496
497 DIG-labeled riboprobes were generated using 2ul of PCR template with the Roche DIG RNA
498 Labeling Kit (T7) (Sigma aldrich, SKU 11277073910)
499 Whole-mount imaging was carried out using a Zeiss Axioscope2 microscope. Embryos were
500 imaged in a 2.5% glycerol solution.
501

502 **Confocal microscopy**

503 <u>Dorsal view time-lapse microscopy</u>: performed as previously described[60]. Embryos were
504 imaged using a Leica confocal microscope (Leica SP5 TCS 4D) at 15 sec/frame capturing
505 <.5µm of tissue. All fluorescently labeled sections were imaged using a Leica confocal
506 microscope (Leica SP5 TCS 4D).

507 Transverse view time-lapse microscopy: performed as described previously[60], with the
508 exception that the embryos were oriented anterior side against the glass. Embryos were
509 imaged using a Zeiss confocal microscope (Zeiss 900 LSM with Airyscan 2), at 20X.
510

511 **Data Quantification**

512 Medial-most-p63-positive-domain migration, Figure 1N: For each hemisphere of a tissue
513 section, the distance between the medial-most p63 positive nucleus and the midline was
514 manually scored. For each embryo, measurements were taken from tissue sections ranging
515 along the anterior-posterior axis of the forebrain.
516
517 Deep layer cell morphology measurements, Figure 3: Cells were manually scored from non-
518 projected z-stack images, where cellular outlines were visually determined from the mGFP
519 signal. Cells were labeled as neuroectoderm NF cells based on the fan-like pattern of their
520 basal projections in contact with the non-neural ectoderm. All other cells scored were within
521 the morphologically distinct eye vesicle and were labeled as eye field cells. Neural ectoderm
522 NF cells and eye field cells are not morphologically distinguishable at the 2 somitic stage and
523 thus were not given cell type identities at that developmental stage.
524

525 Medial hinge cell morphology measurements, Figure 5C: Cells were manually scored from
526 non-projected z-stack images of the overlay between the labeled actin cytoskeleton
527 (phalloidin) and nucleus (DAPI, not shown in Figure 5) channels. Cellular outlines were
528 visually determined from the phalloidin signal. For the nuclear position measurement (Figure
529 5c3), the distance from the dorsal edge of the nucleus to the basal membrane of the cell was
530 scored and divided by the total cell length.

531 Cell ratcheting, Figure 6 a1,a2,b1,b2: Live movie z-stacks for the first 35 minutes (~2-4
532 somites, n=2) of each movie were max projected and cropped so the midline of the tissue
533 horizontally bisected the image frame. The mGFP signal was then inverted and thresholded
534 to produce a binary image. Measurements for individual cell surface areas were captured
535 using the magic wand tool in ImageJ for every frame (15 seconds) until the cell left the field of
536 view. Plotted on the x-axis is the order of frame measurements (frame 0, frame 1, frame 2,...)
537 divided by the total number of frames for which that cell was scored to standardize between 0
538 and 1. Plotted on the y-axis, the initial value of each cell's surface area was subtracted from
539 all measurements for that cell to initialize surface area's to zero. The data was binned
540 (bins=50) to obtain median measurements and confidence intervals. Cells that underwent
541 mitosis anytime during the movie were excluded. Cells were labeled as MHP if their surface
542 area centroid from the first frame (t=0) was +- 20 μm from the midline with MHP-adjacent
543 cells being labeled as such if their centroid was > +-20 μm from the midline.
544
545 Dorsal view movies of apical surface area oscillations: An oscillation was defined as a cycle
546 of constriction and then expansion or vice versa. For a given cell, constriction or expansion
547 was determined by the difference between surface areas for two sequential time frames,
548 where frame_1_surface_area - frame_2_surface_area > 0 was scored as constricting and < 0
549 was scored as expanding.
550
551 Transverse view movies of cell shape changes: Movies were manually scored at each time
552 frame to measure the following parameters (n=2, data shown for Supplemental movie 1 only).
553 Neural groove formation was calculated as the angle formed by the dorsal-most medial tissue

554 (Figure 8G); optic vesicle angle was measured as the angle formed by the outline of the optic
555 vesicle as it forms (Figure 8H); NF basal angle was calculated as the angle formed by the
556 basal surface of NF cells (Figure 8I); NF elevation was measured as the distance between
557 the basal side of NF cells and the apical side of MHP cells (Figure 8J). As the NFs elevate,
558 that distance decreases and eventually becomes negative as the NFs elevate above the
559 MHP. Finally, the distance between the NFs was measured as the distance between the
560 basal side of NF cells, as they migrate towards the midline (Figure 8K).
561
562 *emx3 in situ* hybridization measurements, Figure 10C: The distance between the lateral
563 edges of the posterior-most extent of the emx3 domain was manually scored for each
564 embryo.
565
566 **Statistical Analysis**
567 The Mann-Whitney U test was used for all significance testing. The python function
568 scipy.stats.mannwhitneyu(alternative='two-sided') was used to calculate the test statistic and
569 P-value for each significance test. Graphs were generated using the python Seaborn
570 package with the following functions: seaborn.boxplot(), seaborn.lmplot(), seaborn.violinplot(),
571 seaborn.lineplot().
572
573 **Data availability**
574 The authors declare that all data supporting the findings of this study are available within the
575 article and its supplementary information files or from the corresponding author upon
576 reasonable request.

577 **REFERENCES**

578 1. Copp, A. J., Greene, N. D. E. & Murdoch, J. N. Dishevelled: linking convergent extension
579 with neural tube closure. *Trends Neurosci.* **26**, 453–455 (2003).
580 2. Keller, R. Shaping the vertebrate body plan by polarized embryonic cell movements.
581 *Science* **298**, 1950–1954 (2002).
582 3. Copp, A. J., Greene, N. D. E. & Murdoch, J. N. The genetic basis of mammalian
583 neurulation. *Nat. Rev. Genet.* **4**, 784–793 (2003).
584 4. Morriss-Kay, G. M. Growth and development of pattern in the cranial neural epithelium of
585 rat embryos during neurulation. *J Embryol Exp Morphol* **65 Suppl**, 225–241 (1981).
586 5. Baker, P. C. & Schroeder, T. E. Cytoplasmic filaments and morphogenetic movement in
587 the amphibian neural tube. *Dev. Biol.* **15**, 432–450 (1967).
588 6. Sadler, T. W., Greenberg, D., Coughlin, P. & Lessard, J. L. Actin distribution patterns in
589 the mouse neural tube during neurulation. *Science* **215**, 172–174 (1982).
590 7. Morriss-Kay, G. & Tuckett, F. The role of microfilaments in cranial neurulation in rat
591 embryos: effects of short-term exposure to cytochalasin D. *J Embryol Exp Morphol* **88**,
592 333–348 (1985).
593 8. Schoenwolf, G. C., Folsom, D. & Moe, A. A reexamination of the role of microfilaments in
594 neurulation in the chick embryo. *The Anatomical Record* **220**, 87–102 (1988).
595 9. Ybot-Gonzalez, P. & Copp, A. J. Bending of the neural plate during mouse spinal
596 neurulation is independent of actin microfilaments. *Dev. Dyn.* **215**, 273–283 (1999).
597 10. Kinoshita, N., Sasai, N., Misaki, K. & Yonemura, S. Apical accumulation of Rho in the
598 neural plate is important for neural plate cell shape change and neural tube formation.
599 *Mol. Biol. Cell* **19**, 2289–2299 (2008).
600 11. Hildebrand, J. D. & Soriano, P. Shroom, a PDZ domain-containing actin-binding protein, is
601 required for neural tube morphogenesis in mice. *Cell* **99**, 485–497 (1999).
602 12. Xu, W., Baribault, H. & Adamson, E. D. Vinculin knockout results in heart and brain
603 defects during embryonic development. *Development* **125**, 327–337 (1998).
604 13. Haigo, S. L., Hildebrand, J. D., Harland, R. M. & Wallingford, J. B. Shroom induces apical
605 constriction and is required for hingepoint formation during neural tube closure. *Curr. Biol.*
606 **13**, 2125–2137 (2003).
607 14. Itoh, K., Ossipova, O. & Sokol, S. Y. GEF-H1 functions in apical constriction and cell
608 intercalations and is essential for vertebrate neural tube closure. *J. Cell. Sci.* **127**, 2542–
609 2553 (2014).
610 15. Rolo, A., Skoglund, P. & Keller, R. Morphogenetic movements driving neural tube closure
611 in Xenopus require myosin IIB. *Developmental Biology* **327**, 327–338 (2009).
612 16. Lawson, A., Anderson, H. & Schoenwolf, G. C. Cellular mechanisms of neural fold
613 formation and morphogenesis in the chick embryo. *Anat. Rec.* **262**, 153–168 (2001).
614 17. Colas, J. F. & Schoenwolf, G. C. Towards a cellular and molecular understanding of
615 neurulation. *Dev. Dyn.* **221**, 117–145 (2001).
616 18. Pyrgaki, C., Trainor, P., Hadjantonakis, A.-K. & Niswander, L. Dynamic imaging of
617 mammalian neural tube closure. *Dev. Biol.* **344**, 941–947 (2010).
618 19. Ray, H. J. & Niswander, L. A. Dynamic behaviors of the non-neural ectoderm during
619 mammalian cranial neural tube closure. *Dev. Biol.* **416**, 279–285 (2016).
620 20. Rolo, A. *et al.* Regulation of cell protrusions by small GTPases during fusion of the neural
621 folds. *Elife* **5**, e13273 (2016).

21. Geelen, J. A. & Langman, J. Closure of the neural tube in the cephalic region of the mouse embryo. *Anat. Rec.* **189**, 625–640 (1977).
22. Geelen, J. A. & Langman, J. Ultrastructural observations on closure of the neural tube in the mouse. *Anat. Embryol.* **156**, 73–88 (1979).
23. Massarwa, R., Ray, H. J. & Niswander, L. Morphogenetic movements in the neural plate and neural tube: mouse. *Wiley Interdiscip Rev Dev Biol* **3**, 59–68 (2014).
24. Waterman, R. E. Topographical changes along the neural fold associated with neurulation in the hamster and mouse. *Am. J. Anat.* **146**, 151–171 (1976).
25. Criley, B. B. Analysis of embryonic sources and mechanims of development of posterior levels of chick neural tubes. *J. Morphol.* **128**, 465–501 (1969).
26. Griffith, C. M., Wiley, M. J. & Sanders, E. J. The vertebrate tail bud: three germ layers from one tissue. *Anat. Embryol.* **185**, 101–113 (1992).
27. Kimmel, C. B., Ballard, W. W., Kimmel, S. R., Ullmann, B. & Schilling, T. F. Stages of embryonic development of the zebrafish. *Dev. Dyn.* **203**, 253–310 (1995).
28. Papan, C. & Campos-Ortega, J. A. On the formation of the neural keel and neural tube in the zebrafishDanio (Brachydanio) rerio. *Rouxs Arch. Dev. Biol.* **203**, 178–186 (1994).
29. Hong, E. & Brewster, R. N-cadherin is required for the polarized cell behaviors that drive neurulation in the zebrafish. *Development* **133**, 3895–3905 (2006).
30. Strähle, U. & Blader, P. Early neurogenesis in the zebrafish embryo. *FASEB J.* **8**, 692–698 (1994).
31. Reichenbach, A., Schaaf, P. & Schneider, H. Primary neurulation in teleosts--evidence for epithelial genesis of central nervous tissue as in other vertebrates. *J Hirnforsch* **31**, 153–158 (1990).
32. Miyayama, Y. & Fujimoto, T. Fine morphological study of neural tube formation in the teleost, Oryzias latipes. *Okajimas Folia Anat Jpn* **54**, 97–120 (1977).
33. Lowery, L. A. & Sive, H. Strategies of vertebrate neurulation and a re-evaluation of teleost neural tube formation. *Mech. Dev.* **121**, 1189–1197 (2004).
34. Schmidt, R., Strähle, U. & Scholpp, S. Neurogenesis in zebrafish - from embryo to adult. *Neural Dev* **8**, 3 (2013).
35. Cearns, M. D., Escuin, S., Alexandre, P., Greene, N. D. E. & Copp, A. J. Microtubules, polarity and vertebrate neural tube morphogenesis. *J. Anat.* **229**, 63–74 (2016).
36. Yamaguchi, Y. & Miura, M. How to form and close the brain: insight into the mechanism of cranial neural tube closure in mammals. *Cell. Mol. Life Sci.* **70**, 3171–3186 (2013).
37. Ivanovitch, K., Cavodeassi, F. & Wilson, S. W. Precocious acquisition of neuroepithelial character in the eye field underlies the onset of eye morphogenesis. *Dev. Cell* **27**, 293–305 (2013).
38. England, S. J., Blanchard, G. B., Mahadevan, L. & Adams, R. J. A dynamic fate map of the forebrain shows how vertebrate eyes form and explains two causes of cyclopia. *Development* **133**, 4613–4617 (2006).
39. Viktorin, G., Chiuchitu, C., Rissler, M., Varga, Z. M. & Westerfield, M. Emx3 is required for the differentiation of dorsal telencephalic neurons. *Dev. Dyn.* **238**, 1984–1998 (2009).
40. Schroeder, T. E. Neurulation in Xenopus laevis. An analysis and model based upon light and electron microscopy. *J Embryol Exp Morphol* **23**, 427–462 (1970).
41. Suzuki, M., Morita, H. & Ueno, N. Molecular mechanisms of cell shape changes that contribute to vertebrate neural tube closure. *Dev. Growth Differ.* **54**, 266–276 (2012).

667 42. Smith, J. L. & Schoenwolf, G. C. Cell cycle and neuroepithelial cell shape during bending
668 of the chick neural plate. *Anat. Rec.* **218**, 196–206 (1987).
669 43. Smith, J. L. & Schoenwolf, G. C. Role of cell-cycle in regulating neuroepithelial cell shape
670 during bending of the chick neural plate. *Cell Tissue Res.* **252**, 491–500 (1988).
671 44. Lee, J.-Y. & Harland, R. M. Endocytosis is required for efficient apical constriction during
672 Xenopus gastrulation. *Curr. Biol.* **20**, 253–258 (2010).
673 45. Gutzman, J. H., Sahu, S. U. & Kwas, C. Non-muscle myosin IIA and IIB differentially
674 regulate cell shape changes during zebrafish brain morphogenesis. *Dev. Biol.* **397**, 103–
675 115 (2015).
676 46. Araya, C. *et al.* Cdh2 coordinates Myosin-II dependent internalisation of the zebrafish
677 neural plate. *Sci Rep* **9**, 1835 (2019).
678 47. Karfunkel, P. The activity of microtubules and microfilaments in neurulation in the chick. *J.*
679 *Exp. Zool.* **181**, 289–301 (1972).
680 48. Lee, C., Scherr, H. M. & Wallingford, J. B. Shroom family proteins regulate gamma-tubulin
681 distribution and microtubule architecture during epithelial cell shape change.
682 *Development* **134**, 1431–1441 (2007).
683 49. Sawyer, J. M. *et al.* Apical constriction: a cell shape change that can drive
684 morphogenesis. *Dev. Biol.* **341**, 5–19 (2010).
685 50. Martin, A. C., Kaschube, M. & Wieschaus, E. F. Pulsed contractions of an actin-myosin
686 network drive apical constriction. *Nature* **457**, 495–499 (2009).
687 51. Martin, A. C. & Goldstein, B. Apical constriction: themes and variations on a cellular
688 mechanism driving morphogenesis. *Development* **141**, 1987–1998 (2014).
689 52. Solon, J., Kaya-Copur, A., Colombelli, J. & Brunner, D. Pulsed forces timed by a ratchet-
690 like mechanism drive directed tissue movement during dorsal closure. *Cell* **137**, 1331–
691 1342 (2009).
692 53. Suzuki, M. *et al.* Distinct intracellular Ca2+ dynamics regulate apical constriction and
693 differentially contribute to neural tube closure. *Development* **144**, 1307–1316 (2017).
694 54. McShane, S. G. *et al.* Cellular basis of neuroepithelial bending during mouse spinal
695 neural tube closure. *Dev. Biol.* **404**, 113–124 (2015).
696 55. Zohn, I. E., Anderson, K. V. & Niswander, L. The Hectd1 ubiquitin ligase is required for
697 development of the head mesenchyme and neural tube closure. *Dev. Biol.* **306**, 208–221
698 (2007).
699 56. Nikolopoulou, E., Galea, G. L., Rolo, A., Greene, N. D. E. & Copp, A. J. Neural tube
700 closure: cellular, molecular and biomechanical mechanisms. *Development* **144**, 552–566
701 (2017).
702 57. von Trotha, J. W., Campos-Ortega, J. A. & Reugels, A. M. Apical localization of
703 ASIP/PAR-3:EGFP in zebrafish neuroepithelial cells involves the oligomerization domain
704 CR1, the PDZ domains, and the C-terminal portion of the protein. *Dev. Dyn.* **235**, 967–
705 977 (2006).
706 58. Strehlow, D., Heinrich, G. & Gilbert, W. The fates of the blastomeres of the 16-cell
707 zebrafish embryo. *Development* **120**, 1791–1798 (1994).
708 59. Thisse, C., Thisse, B., Schilling, T. F. & Postlethwait, J. H. Structure of the zebrafish
709 snail1 gene and its expression in wild-type, spadetail and no tail mutant embryos.
710 *Development* **119**, 1203–1215 (1993).
711 60. Jayachandran, P., Hong, E. & Brewster, R. Labeling and imaging cells in the zebrafish
712 hindbrain. *J Vis Exp* (2010) doi:10.3791/1976.

713 **ACKNOWLEDGEMENTS**

714 Funds from Howard Hughes Medical Institute through the UMBC Precollege and
715 Undergraduate Science Education Program supported J. Werner and D. Brooks. Funds from
716 NIH/NIGMS grants # T32-GM055036 and # R25-GM066706 and NSF LSAMP BD grant #
717 1500511 to UMBC supported M. Negesse. Funds from NSF LSAMP grant # 1619676 to
718 UMBC supported J. Johnson. Funds from NIH/NIGMS MARCU*STAR T34 grant # HHS
719 00026 to UMBC supported D. Brooks and A. Caldwell. We thank the following people for their
720 contributions: Tagide deCarvalho for her help with confocal imaging and image processing;
721 Corinne Houart for the *Tg(emx3:YFP)*^{b1200} transgenic line; Jennifer Gutzman for the gift of
722 *myh10* morpholino and Mark Van Doren for his comments on the manuscript.

723 **AUTHOR CONTRIBUTIONS**

724 J.W. and M.N. contributed equally to this study.
725 J.W. designed and performed experiments and carried out data analysis. M.N. carried out
726 experiments and data analysis, annotated movie files and generated illustrations. D.B. and
727 A.C. contributed to the experiments and analysis of cell polarity and myosin function. J.J.
728 contributed to the analysis of myosin function. R.B. oversaw experimental design and
729 analysis and wrote the manuscript.

730 **COMPETING INTERESTS**

731 The authors declare no competing interests

732 **MATERIALS AND CORRESPONDENCE**

733 Rachel Brewster

FIGURES

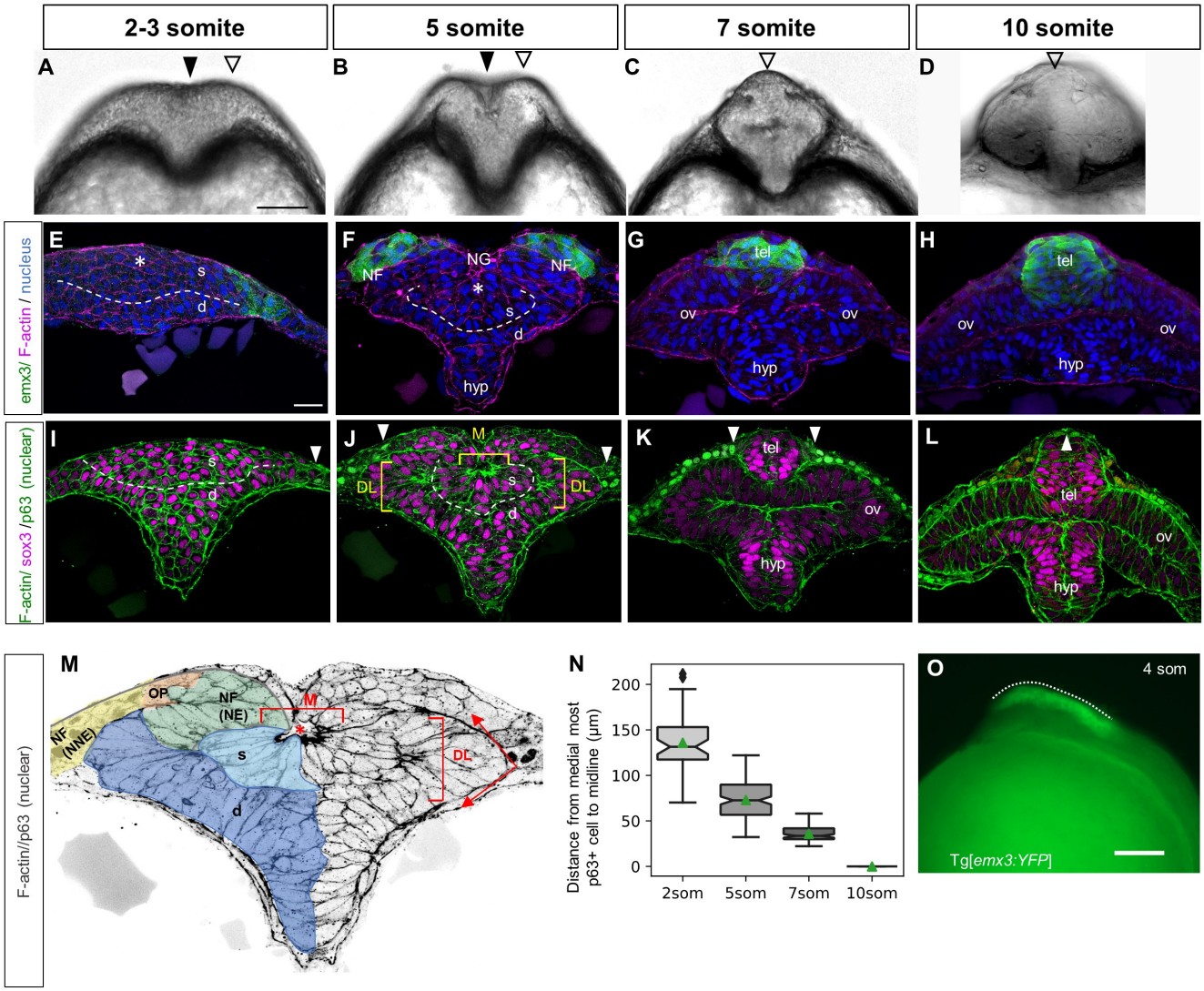

Figure 1. Hingepoints and neural folds contribute to forebrain morphogenesis. (A-D) Optical sections at the level of the forebrain of WT embryos at the 2-3 som (A), 5 som (B), 7 som (C) and 10 som (D) stages. (E-L) Transverse sections through the ANP of 2-3 som(E,I), 5 som (F,J), 7 som (G, K) and 10 som (H, L) embryos. (E-H) Tg[*emx3:YFP*] embryos labeled with anti-GFP (green), phalloidin (F-actin, magenta) and DAPI (nuclei, blue). (I-L) WT embryos labeled with phalloidin (F-actin, green), anti-Sox3 (magenta) and anti-p63 (nuclear label, green). (M) Higher magnification image of panel J, grey scaled to reveal F-actin and p63 and pseudo-colored - color code: light blue: superficial eye field cells, dark blue: deep layer cells that apically constrict to form the optic vesicles, green: neural component of the neural fold, orange: olfactory placode (Sox3/p63-negative cells), yellow: non-neural component of the neural fold. (N) Measurements of neural fold convergence, scored as the distance between the medial-most p63-positive cells on either side of the midline at different developmental stages. Notches depict the 95% confidence interval around the median and the green triangle depicts the distribution mean. 2 som: 48 measurements from 14 embryos, mean= 136; 5 som: 144 measurements from 16 embryos, mean=73.0; 7 som: 87 measurements from 10 embryos, mean=36.0; 10 som: p63 domain is fused, no measurements. Statistical analysis: Mann-Whitney U tests, two-sided; 2 som vs 5 som : P = 1.18e^-21; 2 som vs 7 som : P = 8.35e^-22; 5 som vs 7 som : P = 2.14e^-31. (O) Side view of a 4 som

Tg[*emx3:YFP)* embryo. Abbreviations: s = superficial layer; d = deep layer; NF = neural fold; NG = neural groove; hyp = hypothalamus; tel = telencephalon; ov = optic vesicle; DL = Dorso-lateral hingepoints; M = Medial hingepoint; OP = olfactory placode; NE = neural ectoderm; NNE = non-neural ectoderm. Annotations: black arrowhead = median groove, white open arrowhead = elevated neural fold-like structure, dashed line = separation of the deep and superficial layers; brackets = hingepoints; dotted line = A-P range of the neural folds; white arrowhead = medial-most epidermis; red asterisk = neuropore. Scale bars: A and O= 100 µm, E= 25 µm.

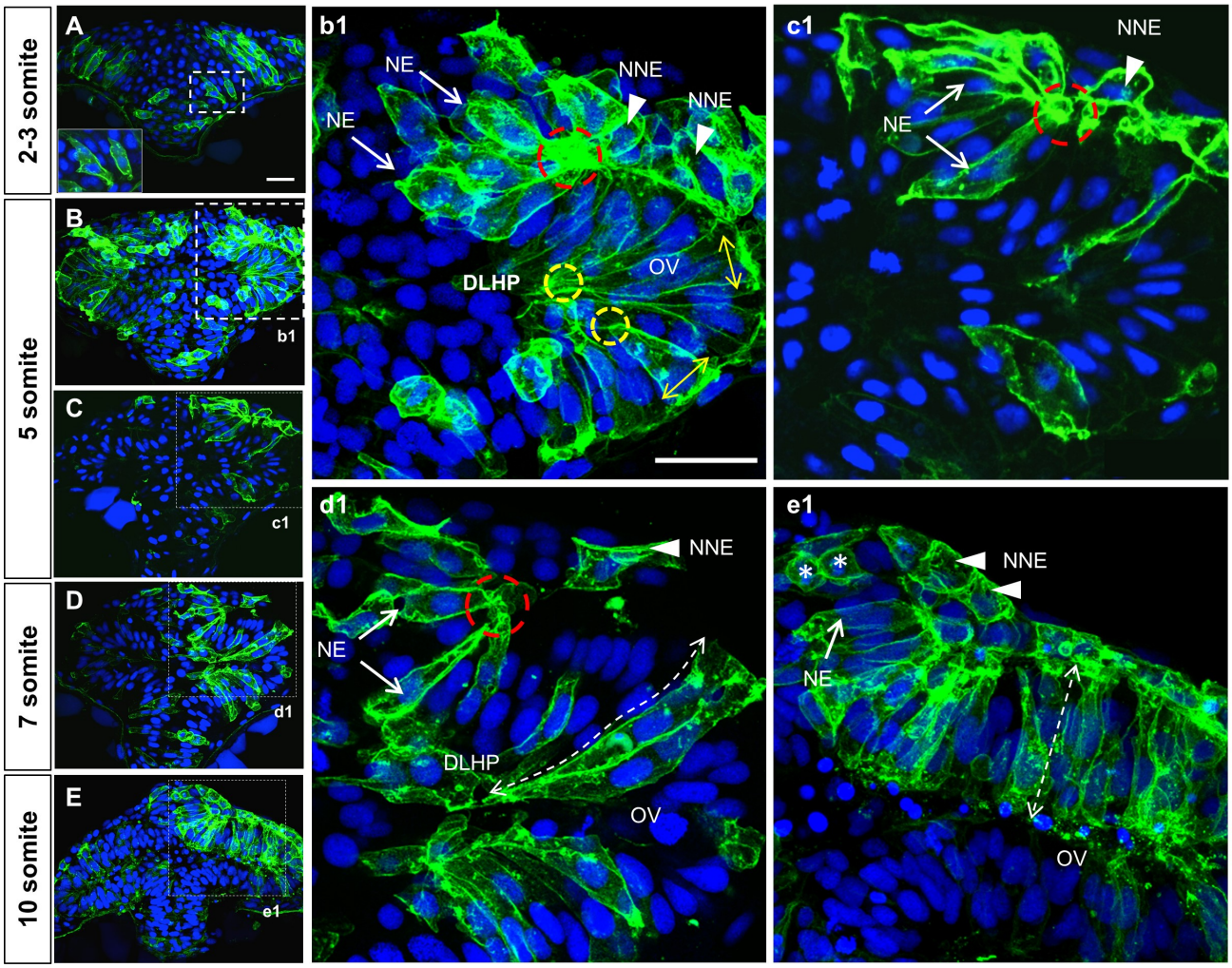

Figure 2. Cell shape changes in the deep layer of the ANP that contribute to DLHP and neural fold formation. (A-E) Transverse section, at the level of the forebrain, of embryos at the 2-3 (A), 5 (B, b1, C, c1), 7 (D, d1) and 10 (E, e1) somite stages mosaically-expressing mGFP (green) and labeled with the nuclear marker DAPI (blue). The inset in A is a higher magnification of dashed area in A**.** (b1-e1) Higher magnifications of regions delineated by dotted lines in (A-E). Annotations: red dashed circle = basal constriction of NE component of neural fold; yellow circle = apical constriction of DLHP cells; arrows = NE component of neural fold; arrowheads = NNE component of neural folds; double dashed arrow = elongated deep cells of the optic vesicle, asterisks = dividing cells in the prospective telencephalon. Scale bars: 25 μm in A and b1.

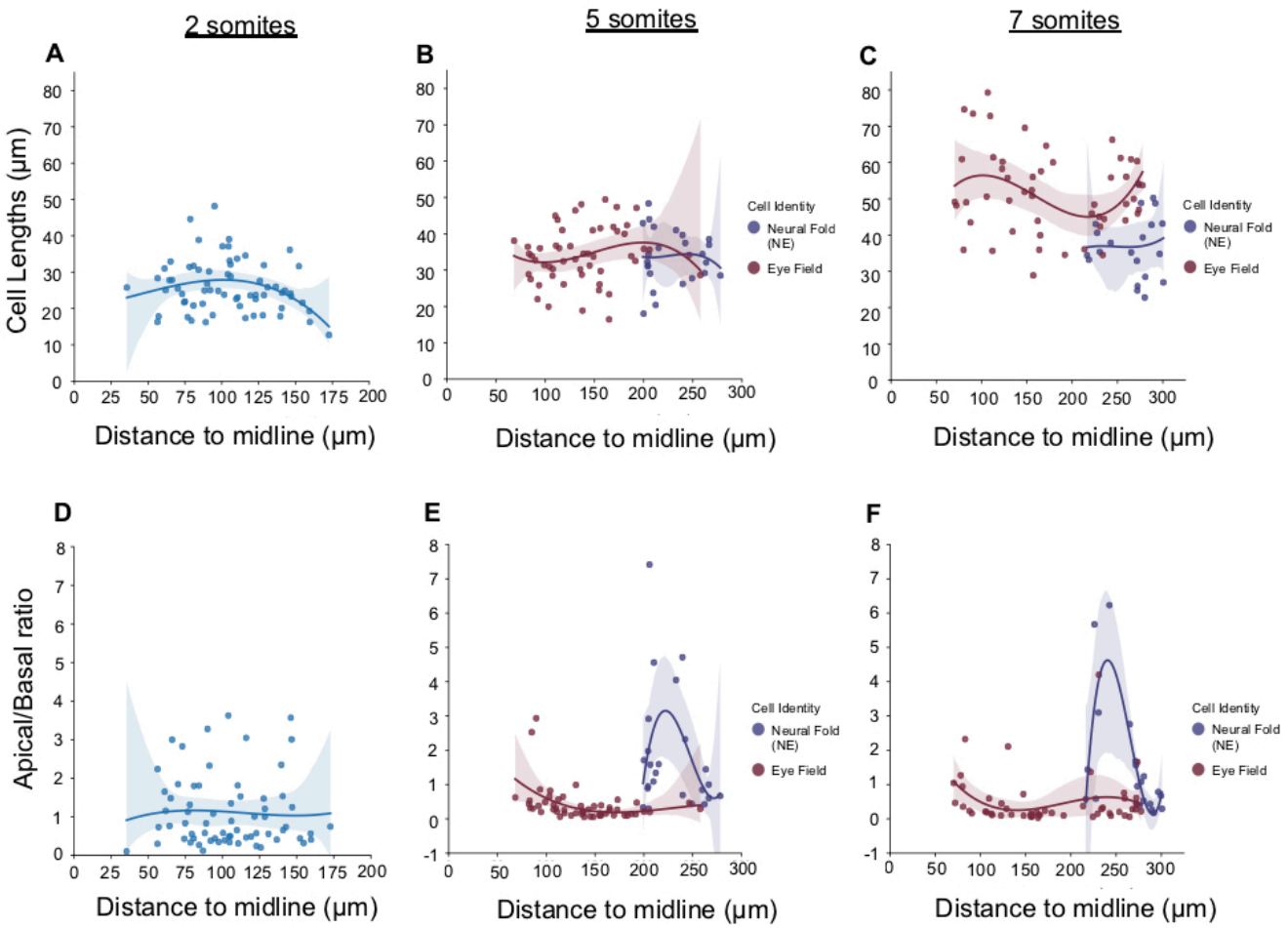

Figure 3. Measurements of cell shape changes in the deep neuroectodermal layer and neural folds. (A-C) Measurements of cell lengths (µM, Y axis) of m-GFP-labeled cells at different positions relative to the ANP midline (µM, X axis). Measurements begin in the region fated to become the optic vesicles. (D-F) Measurements of the apico:basal surface ratio of m-GFP-labeled cells at different positions relative to the ANP midline (µM, X axis). Measurements begin in the region fated to form the optic vesicles. The original scatter plot was fitted to a 3rd degree polynomial. Confidence intervals for the polynomial are 95% and were calculated with bootstrap sampling (n=1000). Color code: blue = neuroectodermal cells of the deep layer of 2 som stage embryos that are not yet identifiable based on cellular morphology; red = cells that form the optic vesicles; blue = cells that form the neuroectodermal component of the neural folds.

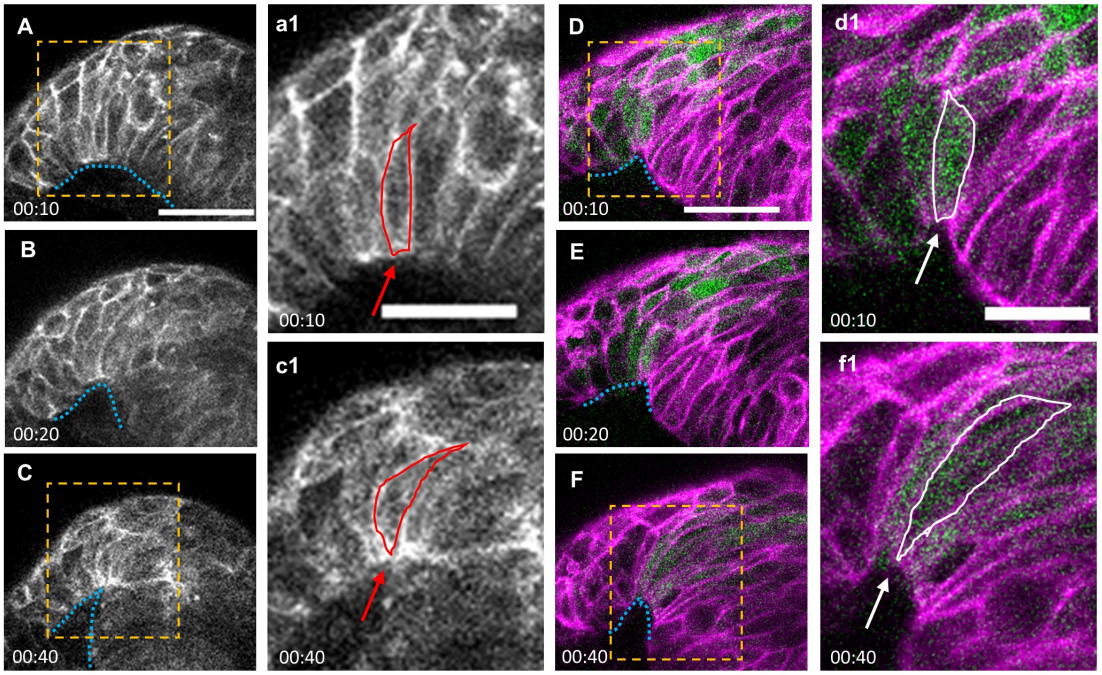

Figure 4. Dynamics of neural fold formation. A-F. Time lapse movie frames of the ANP, from a transverse view. A-C. Still frames of an embryo expressing membrane Kaede (mKaede). D-F. Still frames of a Tg[*emx3:YFP*] embryo expressing membrane RFP (mRFP, pseudo labeled magenta) and YFP (green). Yellow boxes in A, C, D and F identify magnified areas in a1, c1, d1 and f1. Annotations: blue dotted line: outlines the basal side of the neural folds; red and white lines identify individual neural fold cells; arrows: indicate narrowing surface in neural folds cells. Scale bars: 50 μm in A and D; 25 μm in a1 and d1.

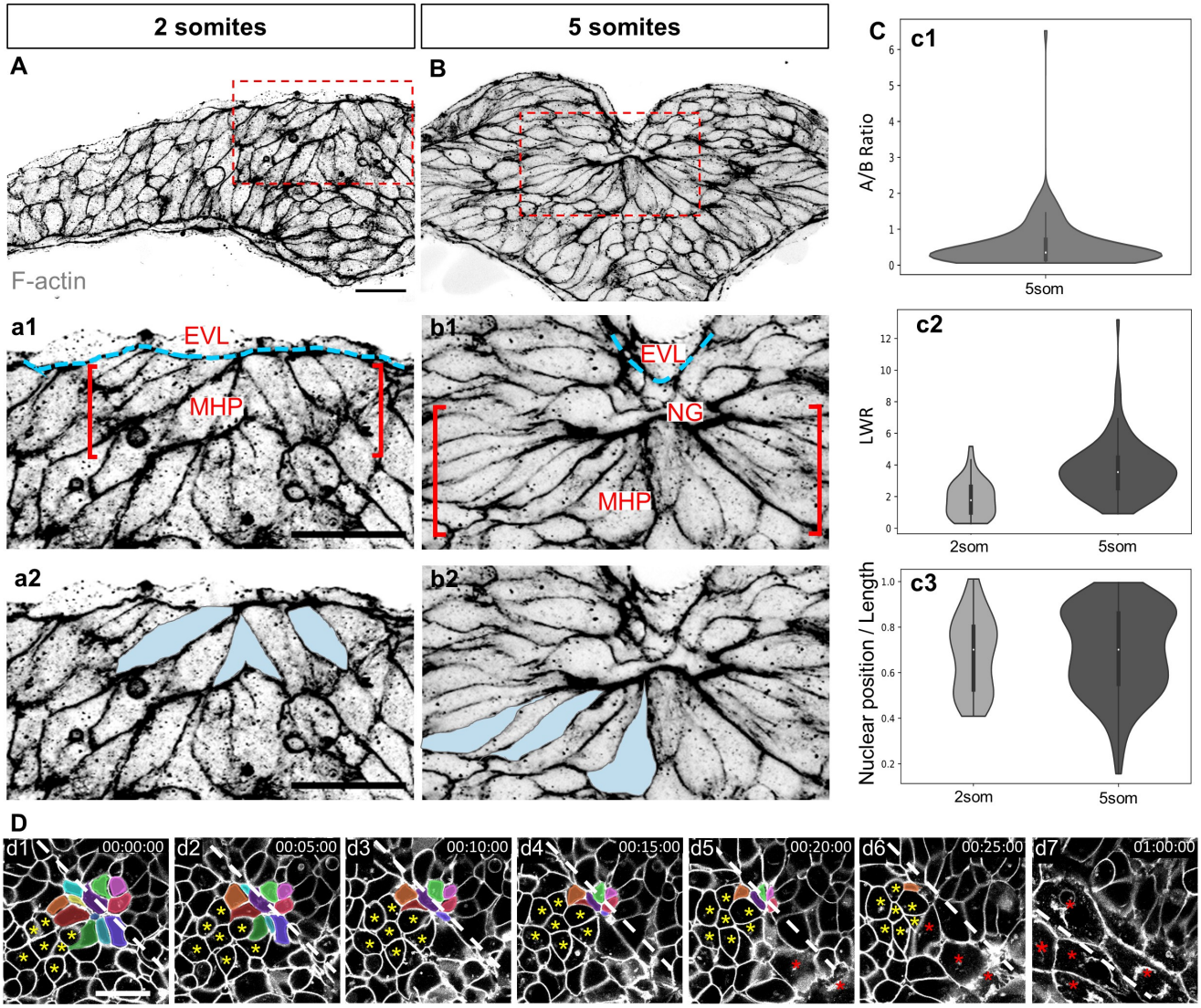

Figure 5. Apical constriction of MHP cells. (A-b2) Transverse sections through the ANP at the 2 (A, a1, a2) and 5 (B, b1, b2) som stages labeled with phalloidin (shown in greyscale). (a1-b2) are higher magnifications of the boxed areas in A and B, revealing the organization of the medial ANP (a1, b1) and the shape of individual MHP cells pseudo-colored in blue (a2, b2). (C) Quantitation of cell shape changes. Boxplot elements depict quartiles with the centerline depicting the median. (c1) Measurements of apical:basal surface ratio at 5 som (n= 115 cells from 4 embryos, mean=0.548). (c2) Measurement of length-to-width (LWR) ratio at 2 som (n= 47 cells from 5 embryos, mean=1.88) and 5 som (same cells as in c1, mean=3.70). A Mann-Whitney two-sided U Test revealed that the LWR increase between 2 som and 5 som is statistically significant (P = 7.80e^-11). (c3) Relative position of nucleus at 2 and 5 som measured in the same cell populations (c2). Mean nuclear position/cell length (0.682 at 2 som vs 0.696 at 5 som) is not statistically significant using a Mann Whitney U test (P=0.419). (D) Still frames of time lapse movie of m-GFP labeled embryo imaged from a dorsal view. Individual MHP cells are pseudo-colored, A cluster of cells adjacent to the MHP is indicated with yellow asterisks and EVL cells are labeled with red asterisks. Abbreviations: EVL = enveloping layer; MHP = medial hingepoint; NG = neural groove. Annotations: white dashed line= midline, red brackets = MHP region, blue dashed lines = outlines EVL, yellow asterisks: cells adjacent to MHP, red asterisks: EVL cells. Scale bars: 25 µm in A, a1 and a2; 10 µm in d1.

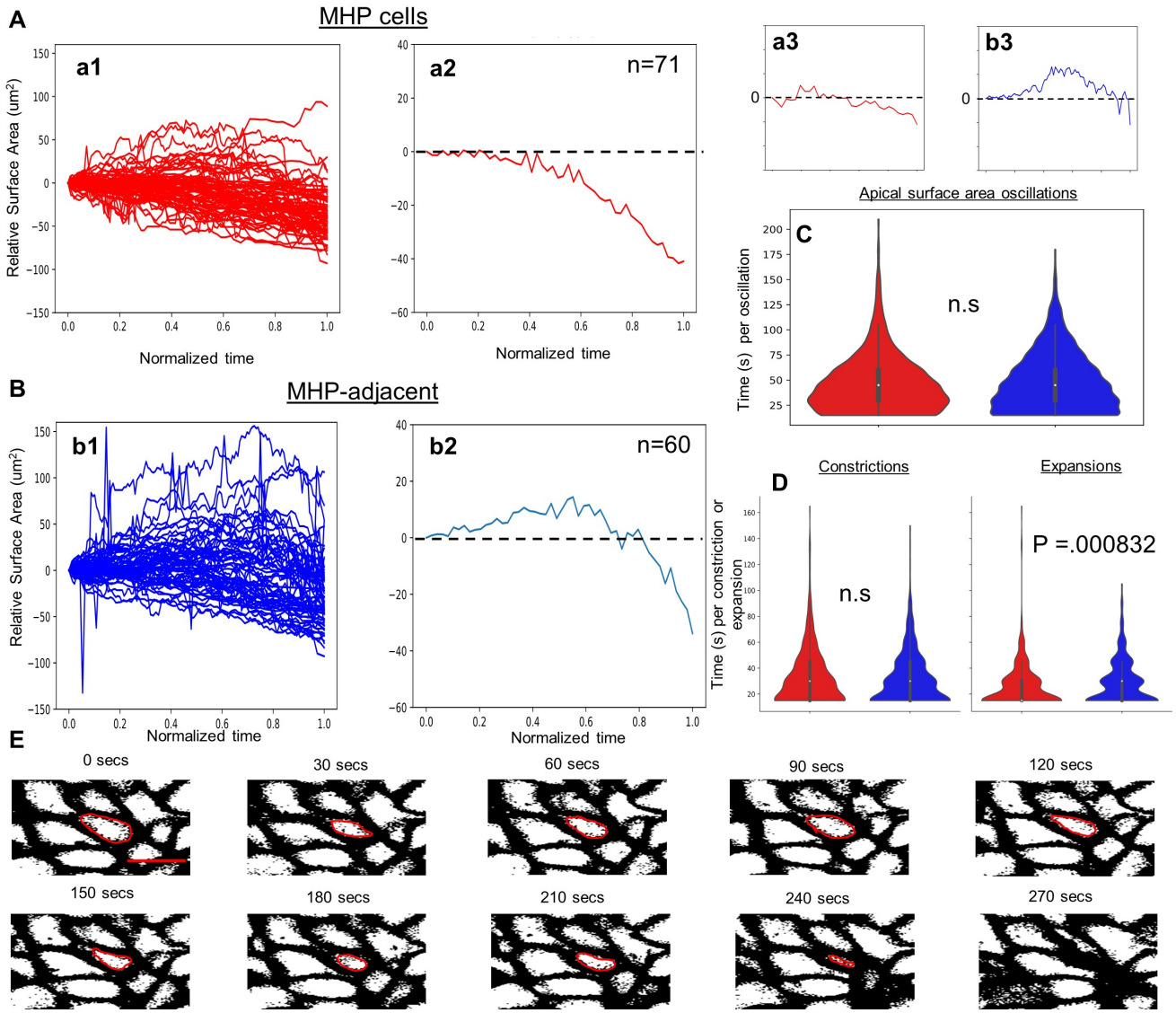

Figure 6. Oscillatory constriction with decreasing amplitude reduces the apical surface of MHP cells. (A) Measurements of medial, MHP cells. (a1) Relative apical surface areas over time for individual MHP cells. (a2) Median values of MHP relative apical surface areas over time, 95% confidence interval, n=71. (a3) Representative trace of relative apical surface area over time for an individual MHP cell**.** (B) Measurements of MHP-adjacent cells. (b1) Relative apical surface areas over time for individual MHP-adjacent cells. (b2) Median values of MHP-adjacent relative apical surface areas over time, 95% confidence interval. (b3) Representative trace of relative apical surface area over time for an individual MHP-adjacent cell. (C) Distributions of the duration of oscillation between two expanded states for MHP cells (red, median of 45 seconds per oscillation) and MHP-adjacent cells (blue, median of 45 seconds per oscillation). No significant difference (two-sided Mann Whitney U test, P=0.293, n=758 MHP cell oscillations, n=1,113 MHP-adjacent oscillations). (D) Distributions of the timing of apical constrictions or expansions for MHP cells (red) and MHP-adjacent cells (blue). There is no significant difference between the two groups for constriction time (two-sided Mann Whitney U test: constrictions, P=0.541, n= 458 MHP cell constrictions, n=640 MHP-adjacent constrictions) but there is a statistically significant difference for expansion time (P = 0.000832, n= 367 MHP-cell expansions, n=596 MHP-adjacent expansions). The median time for individual expansions of MHP and MHP-adjacent cells is 15 and 30 seconds respectively. All boxplot elements depict quartiles with the centerline depicting the median. (E) Still frames of time-lapse movie of m-GFP labeled cells shown in grey-scale. The oscillatory behavior of one cell, outlined in red, is shown over time. Scale bar: 10 μm in c1.

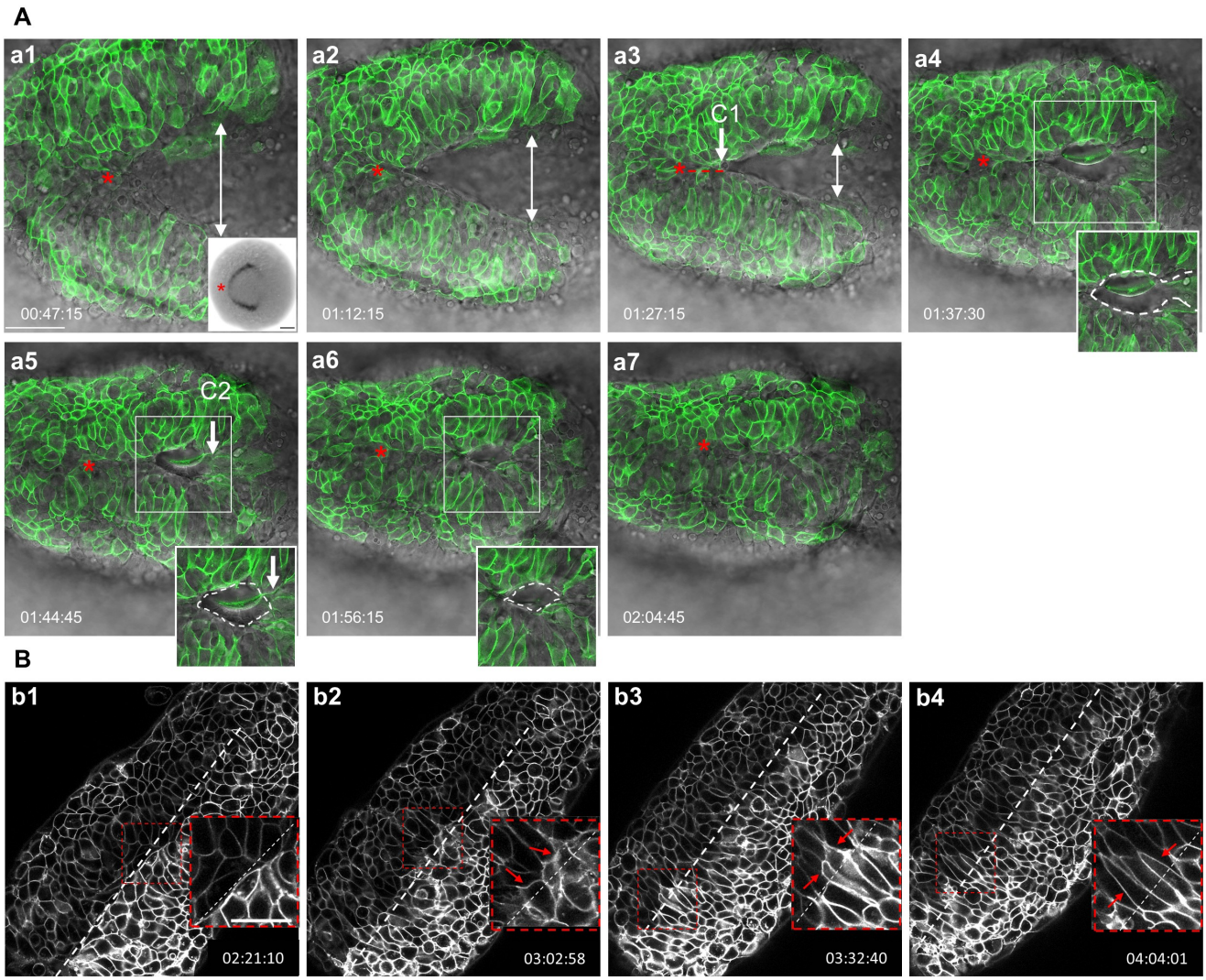

Figure 7. Dynamics of neural fold fusion. (A, a1-a7) Time lapse movie frames of an embryo expressing mosaic GFP, imaged from a dorsal view, showing the initiation of neural tube closure. Images are overlays of the green and brightfield channels. Inset in a1 shows a dorsal view of an *emx3*-labeled embryo. Insets in a4-a6 outline the eye-shaped opening that forms between closure sites one (CP1) and two (CP2) (B) Grey-scale time-lapse movie frames of an mGFP-labeled embryo imaged from a dorsal view, revealing the final stages of neural fold fusion. Insets in the lower right corner of panels b1-b4 are higher magnification views of boxed areas. Abbreviations: C1, C2: closure sites one and two. Annotations: red asterisk: apex of the neural fold arc; red dotted line: synchronous and posteriorly-directed neural fold fusion anterior to closure point one; white double arrows: distance between the neural folds; white dotted oval: eye shaped opening, the corners of which are defined by closure points one and two; white dotted line: embryonic midline; red arrows: filopodia extending across the midline; time-elapse is shown at the bottom of each panel. Scale bars: 50 μm in a1, 100 μm in a1 inset, and 25 μm in b1.

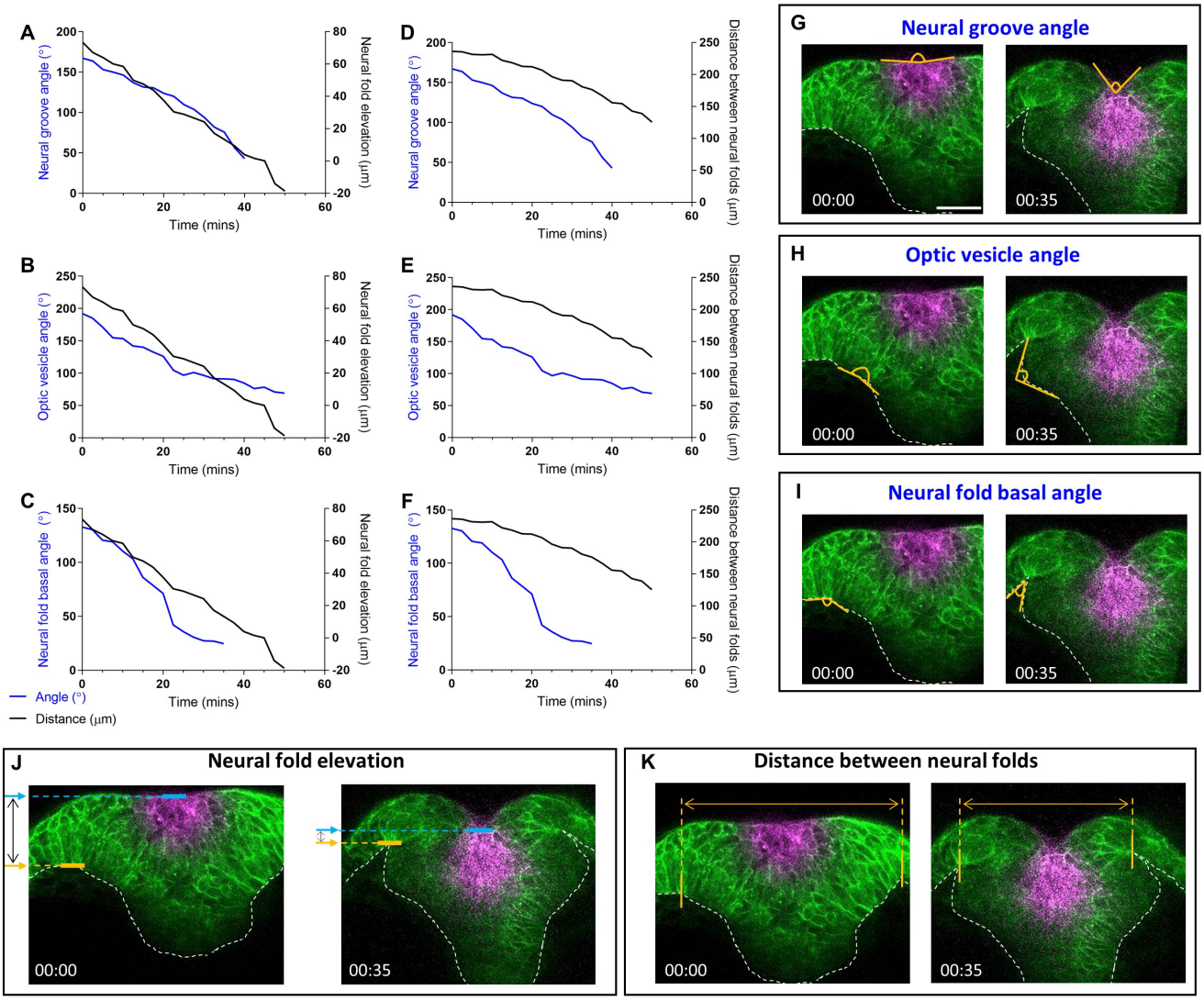

Figure 8. Dynamics of anterior neurulation. A-F. Graphs illustrating the dynamics of neural groove formation (left Y axis, blue line in A and D), optic vesicle angle (left Y axis, blue line in B and E) and neural fold basal angle (left Y axis, blue line in C and F) as compared to neural fold elevation (right Y axis, black line in A-C) and distance between the neural folds (right Y axis, black line in D-F) over time (X axis). G-K. Still frames of an embryo expressing mKaede (green), in which the MHP cells were photoconverted (magenta), showing how the measurements in graphs A-F were acquired, at two discrete time points. G. The neural groove was measured as the angle formed by the dorsal most tissue. H. The optic vesicle angle was measured as the angle formed by the outline of the optic vesicle as it forms. I. The neural fold basal angle was calculated as the angle formed by the basal side of neural fold cells. J. Neural fold elevation was measured as the distance between the basal side of neural fold cells and the apical side of MHP cells. As the neural folds elevate, that distance decreases and eventually becomes negative as the neural folds elevate above the MHP. K. Distance between the neural folds was measured as the distance between the basal side of neural fold cells. Scale bar: 50 µm.

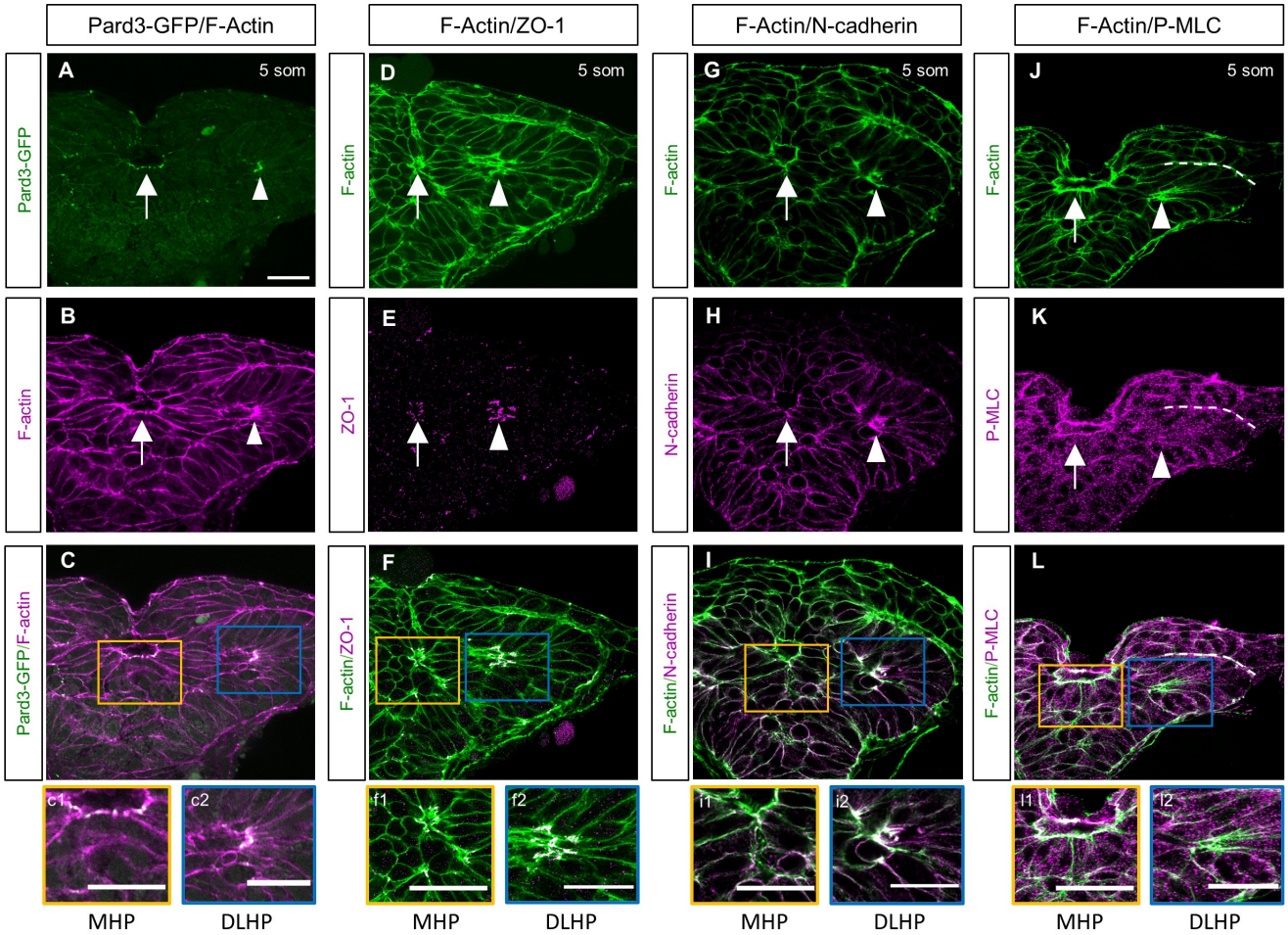

Figure 9. Molecular characterization of the MHP. (A-L). Transverse sections through the ANP at the 5som stage. Embryos double-labeled with Pard3-GFP (green) and phalloidin (F-actin, magenta) (A-c2); ZO-1 (magenta) and F-actin (green) (D-f2); N-cadherin (magenta) and F-actin (green) (G-i2); and with anti-P-MLC (magenta) and F-actin (green) (J-l2).(C, F, I, L) Magenta and green channel overlay. Insets show higher magnification images of the MHP (yellow box) and DLHP (blue box). Annotations: arrow = MHP; arrowhead = DLHP; dotted line (in J-L) = interface between the NE and NNE layers of the neural folds. Scale bars: 25 μm.

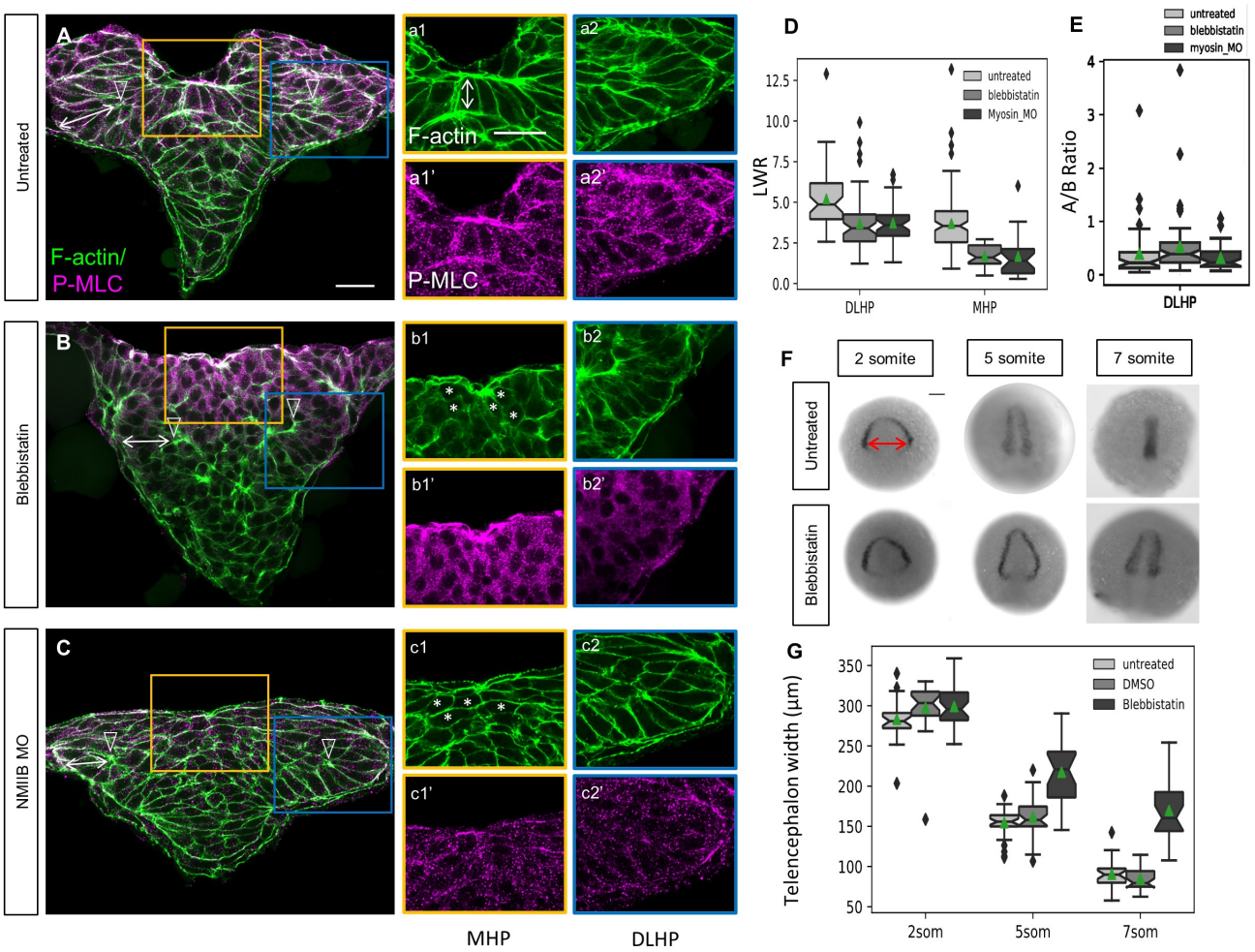

Figure 10. Role of non-muscle myosin II in apical constriction and neural fold convergence. Transverse sections through the ANP of 5 som untreated (A-a2'), blebbistatin-treated (B-b2') and *NMIIB* MO-injected embryos (C-c2'). Embryos were labeled with phalloidin (F-actin, green) and anti-P-MLC (magenta). (D) Length-width ratio distributions for DLHP and MHP cells from untreated, blebbistatin-treated, and *NMIIB* MO-injected embryos. DLHP measurements: untreated: n = 50 cells (5 embryos), mean=5.22; blebbistatin-treated: n = 58 cells (4 embryos), mean=3.70; *NMIIB* MO-injected: n = 38 cells (3 embryos), mean=3.74. MHP measurements: untreated: n=115 cells (4 embryos), mean= 3.70 (same data as in Figure 5 c2); blebbistatin-treated: n= 35 cells (4 embryos), mean=1.70; *NMIIB* MO-injected: n= 24 cells (3 embryos), mean = 1.68. Two-sided Mann Whitney U test: DLHP: untreated vs blebbistatin: P=1.30e^-6; untreated vs *NMIIB* MO-injected: P = 2.14e^-5; MHP: untreated vs blebbistatin: P=3.55e^-12; untreated vs *NMIIB* MO-injected: P = 3.50e^-8. (E) Apical-to-basal length ratios of DLHP cells for untreated, blebbistatin-treated and *NMIIB* MO-injected embryos, same cells quantified as in D. Two-sided Mann Whitney U test: untreated vs blebbistatin-treated P= 0.00665; blebbistatin-treated vs *NMIIB* MO-injected: P=0.00827; untreated vs *NMIIB* MO-injected: P=0.930. (F) Dorsal views of 2, 5 and 7 som embryos untreated or blebbistatin-treated labeled via *in situ* hybridization using an *emx3* riboprobe. (G) Boxplots showing distribution of telencephalon widths (double red arrow in F) according to treatment group. Notches depict the 95% confidence interval around the median and green triangles depict distribution means. 2 som: Untreated: n=26, mean=283.224; DMSO-treated: n= 26, mean=297.727; blebbistatin-treated: n = 34, mean=299.412. 5 som: Untreated: n=33, mean=154.688; DMSO: n=30, mean=161.747; blebbistatin-treated:

885 n=23, mean=217.472. Two-sided Mann Whitney U test: 5 som - untreated vs DMSO: P=0.332; untreated
886 vs blebbistatin-treated: P=1.30e^-7; DMSO-treated vs blebbistatin-treated: P = 3.50e^-6. 7 som: untreated:
887 n=28, mean=90.444; DMSO-treated: n=27, mean 84.855; blebbistatin-treated: n=24, mean= 169.779. Two-
888 sided Mann Whitney U test: 7 som - untreated vs DMSO: P=0.170; untreated vs blebbistatin-treated: P=2.06e^-
889 9; DMSO-treated vs blebbistatin-treated: P = 1.46e^-9. Annotations: double white arrows = cell length in deep
890 layer; open arrowhead = DLHP; asterisks = rounded neuroectodermal cells; red double arrow = posterior-most
891 telencephalon width. Scale bars: 25 μm in A and a1; 100 μm in B.

SUPPLEMENTARY MOVIE LEGENDS

Supplemental Movie 1. MHP cells sink inwards as neural folds elevate. Time lapse imaging of embryo ubiquitously expressing m Kaede (green) that was photo-converted in medial superficial cells that form the MHP (magenta). Annotations: Cyan arrowhead: basal surface of neural fold cells; white arrows: sinking of MHP cells.

Supplemental Movie 2. 3-Dimensional rotation revealing organization of neural fold cells in a 5 som embryo. Transverse section, at the level of the forebrain of a 5 somite embryo mosaically-expressing mGFP.

Supplemental Movie 3. 3-Dimensional rotation revealing organization of neural fold cells in a 7 som embryo. Transverse section, at the level of the forebrain of a 7 somite embryo mosaically-expressing mGFP.

Supplemental Movie 4. Neural fold cells constrict basally as neural folds elevate. Time lapse imaging of Tg[*emx3:YFP*] transgenic embryo ubiquitously expressing mRFP. YFP-positive neural fold cells (green) constrict basally as neural folds elevate. Annotations: Cyan arrow: basal surface of neural fold cells; white lines: telencephalon cells expressing YFP.

Supplemental Movie 5. MHP cells undergo oscillatory constriction with decreasing amplitude. Time lapse imaging of embryo ubiquitously expressing mGFP. Clusters of medial (MHP) constrict apically in an oscillatory manner, in contrast to their lateral neighbors that do not. Annotations: cyan dots = MHP cells; yellow asterisks = MHP-adjacent cells that do not undergo apical constriction, yellow dashed line: midline, red asterisks = EVL cells.

Supplemental Movie 6. Neural tube closure is initiated at two closure points in the forebrain. Time lapse imaging of embryo mosaically-expressing mGFP. The Green and brightfield channels are overlaid to reveal the shape of the neural folds and neural groove. Annotations: red asterisk: apex of the arch shaped neural folds; white dotted line: contour of the eye-shaped opening whose corners are defined by closure points 1 and 2, double headed arrow: width of the neural plate, which decreases over time, white arrows: closure points 1 and 2, respectively.

Supplemental Movie 7. Neural fold cells extend filopodial protrusions across the midline. Time lapse imaging of embryo ubiquitously expressing mGFP. Cells (cyan and magenta) originating from contralateral sides of the ANP extend medially oriented filopodia and transiently interdigitate across the midline (yellow dashed line).

929 **SUPPLEMENTAL FIGURE**

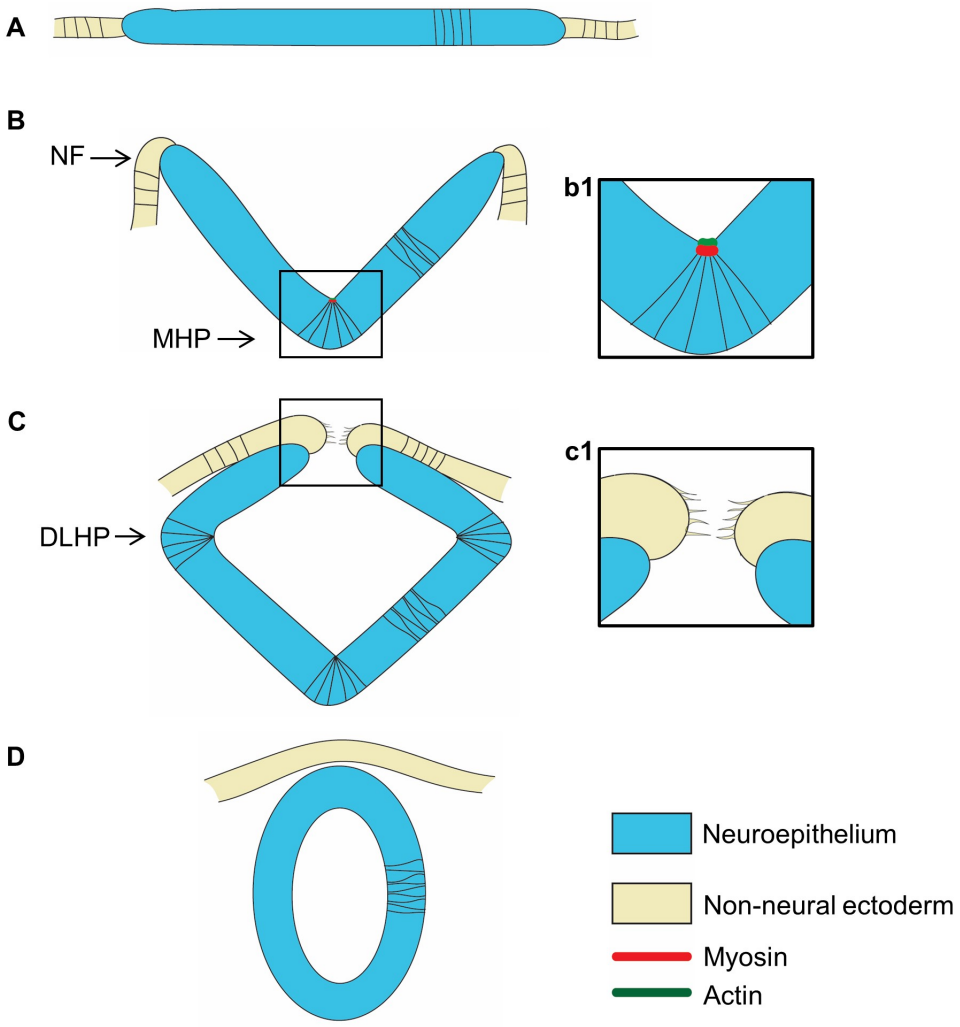

930
931
932 **Supplemental Figure S1. Neurulation in amniotes. Cross sectional illustration of stages of neurulation in**
933 **amniotes.** (A) The neural plate and adjacent non neural ectoderm. (B) Medial hingepoint formation shapes the
934 neural groove and elevates the neural folds. (b1) Illustration of medial hingepoint cells that are apically
935 constricted and enriched for actomyosin at their apex. (C) Dorso-lateral hingepoint formation brings the neural
936 folds in close apposition. (c1) Filopodial extensions establish contact between neural fold cells across the
937 midline. In the mouse forebrain the first contact is established between neuroectodermal cells. (D) The neural
938 folds fuse medially, separating the epidermis from the neural tube. Abbreviations: DLHP = dorso-lateral
939 hingepoint; MHP = medial hingepoint; NF = neural fold.

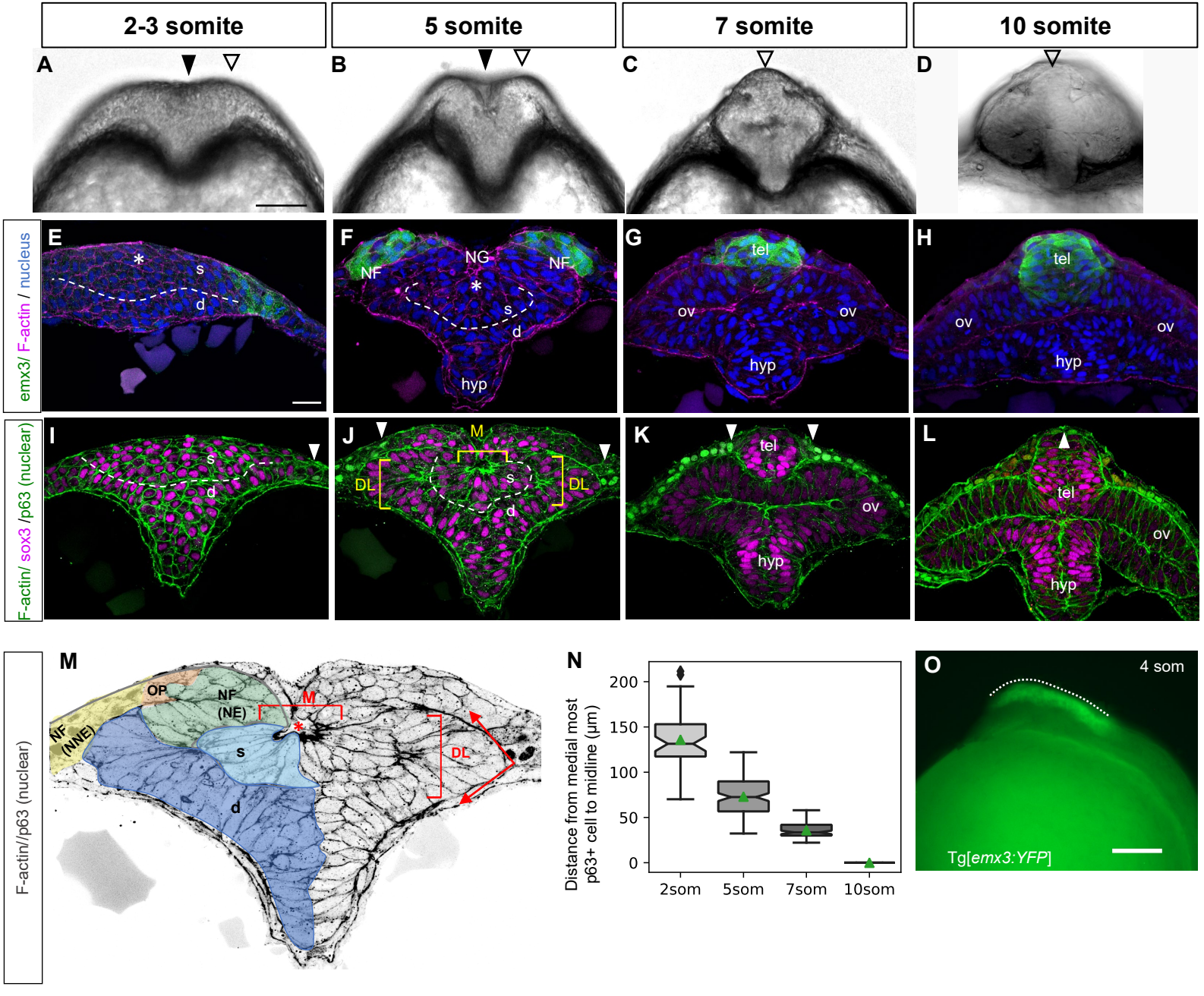
2-3 somite
5 somite
7 somite
10 somite
A
B
C
D
emx3/ F-actin / nucleus
E
F
G
H
s
d
NG
NF
hyp
tel
ov
F-actin/ sox3 /p63 (nuclear)
I
J
K
L
M
DL
F-actin//p63 (nuclear)
OP
NF (NE)
NF (NNE)
N
Distance from medial most p63+ cell to midline (µm)
200
150
100
50
0
2som
5som
7som
10som
O
4 som
Tg[emx3:YFP]

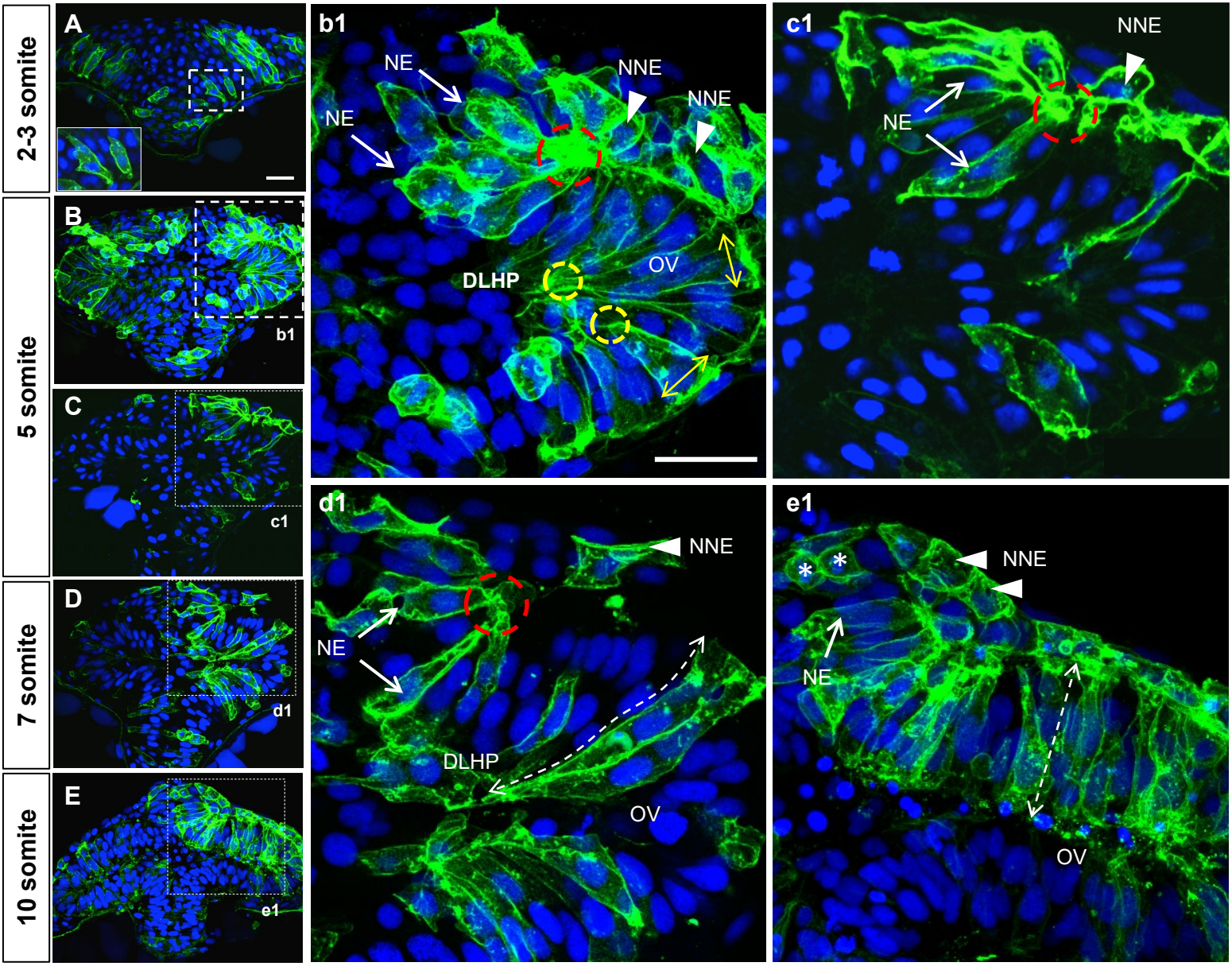
2-3 somite
5 somite
7 somite
10 somite
A
B
b1
C
c1
D
d1
E
e1
NE
NNE
DLHP
OV
*

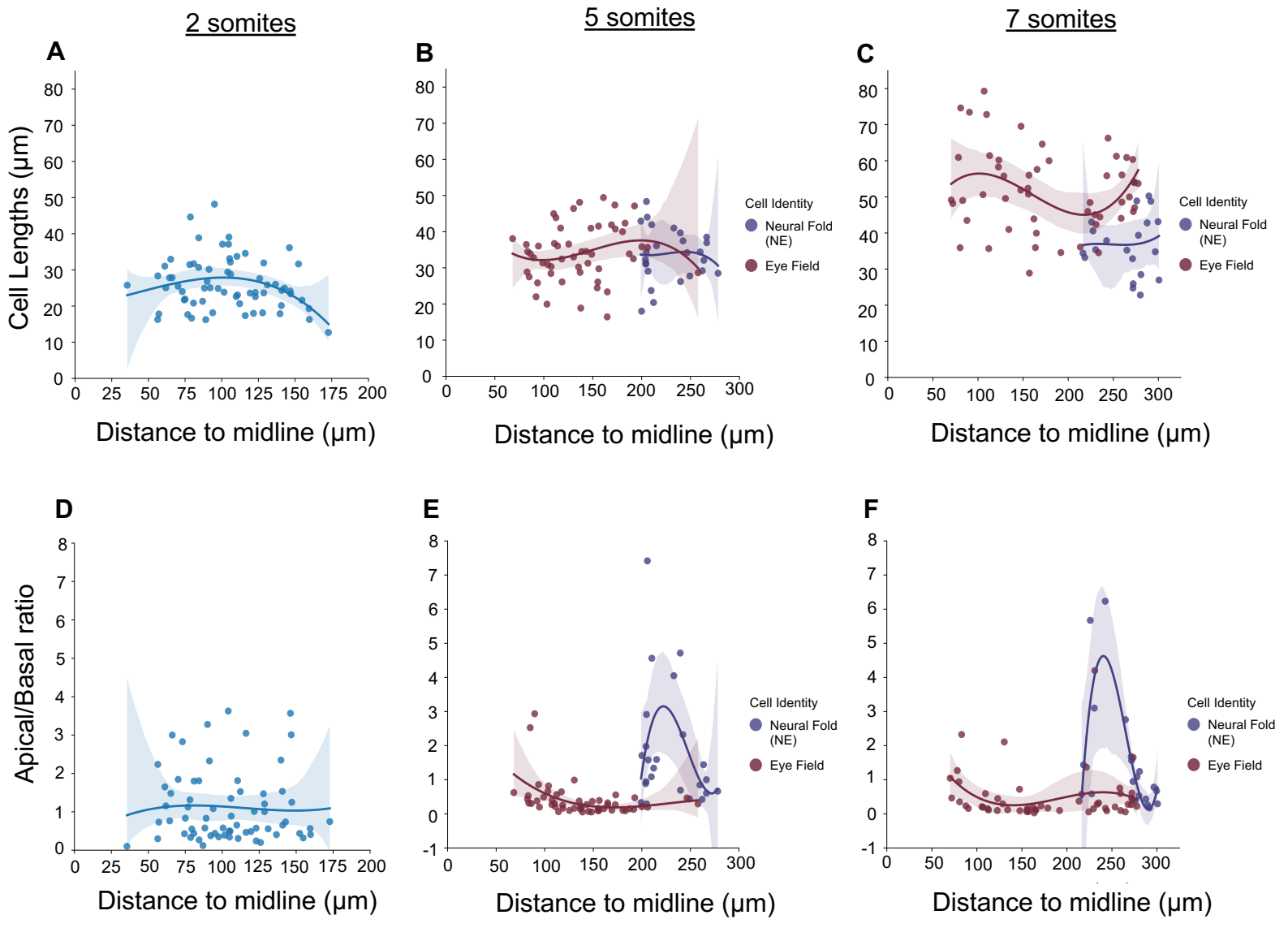
2 somites
5 somites
7 somites
A
B
C
D
E
F
Cell Lengths (µm)
Apical/Basal ratio
Distance to midline (µm)
Cell Identity
Neural Fold (NE)
Eye Field

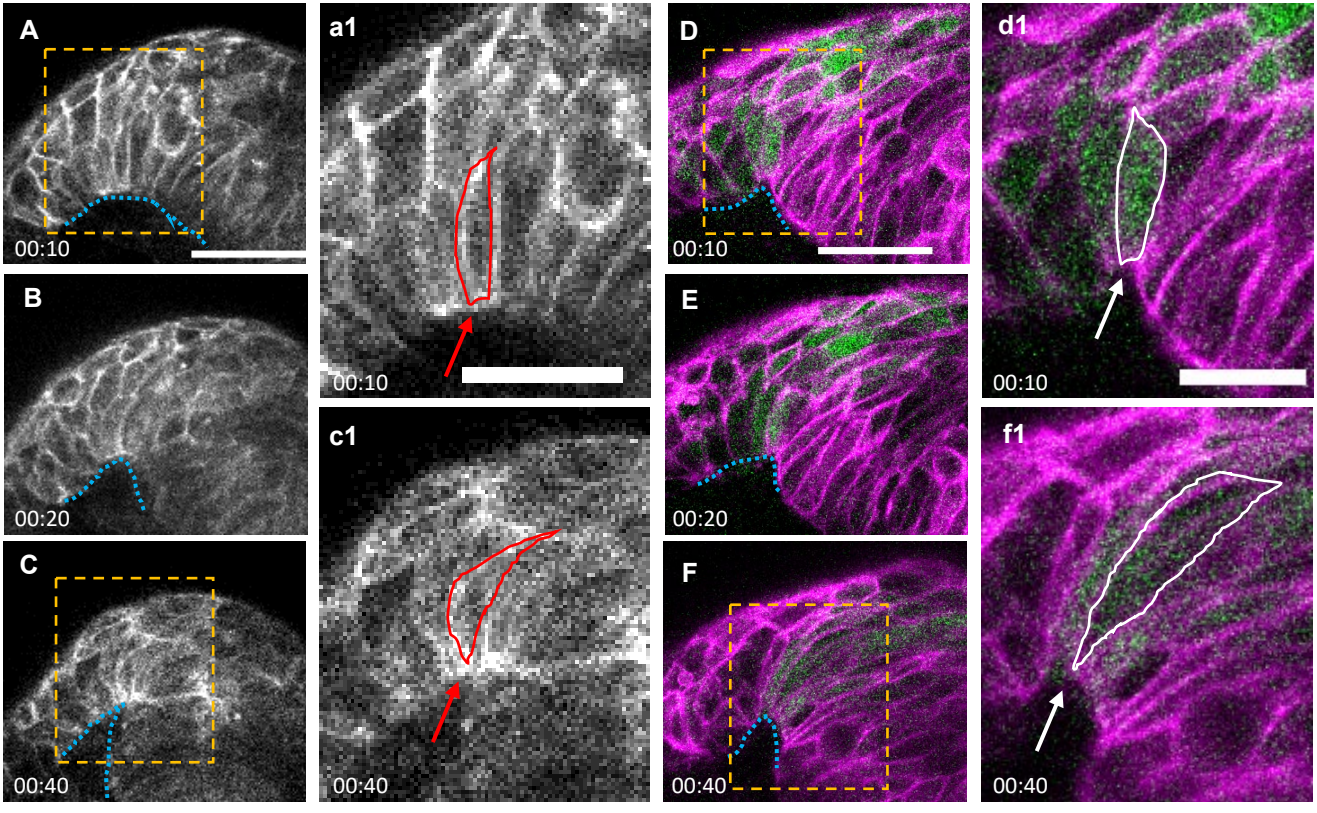
A
00:10
B
00:20
C
00:40
a1
00:10
c1
00:40
D
00:10
E
00:20
F
00:40
d1
00:10
f1
00:40

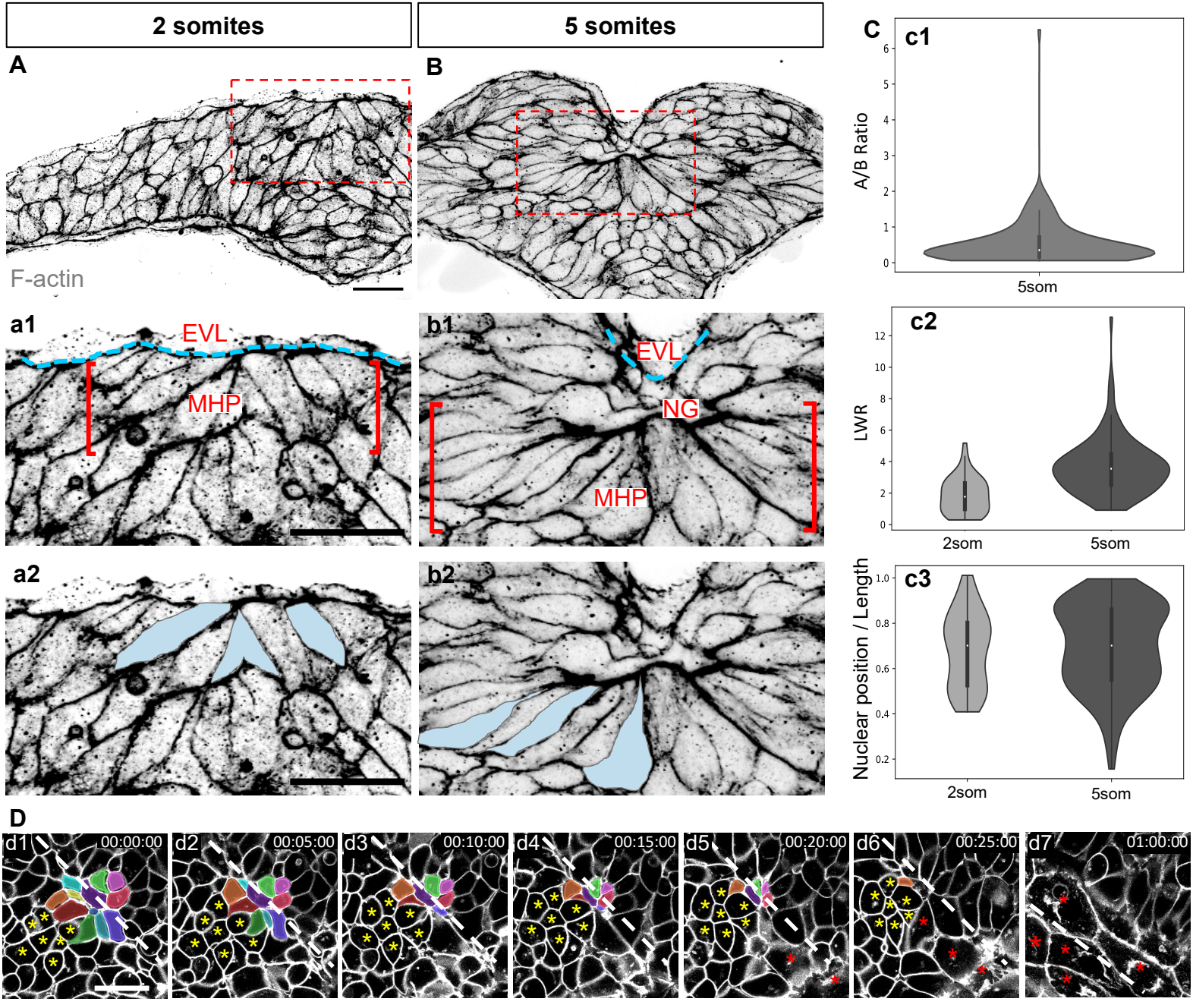
2 somites
5 somites
A
B
F-actin
a1
EVL
MHP
b1
EVL
NG
MHP
a2
b2
C
c1
A/B Ratio
5som
c2
LWR
2som
5som
c3
Nuclear position / Length
2som
5som
D
d1
00:00:00
d2
00:05:00
d3
00:10:00
d4
00:15:00
d5
00:20:00
d6
00:25:00
d7
01:00:00

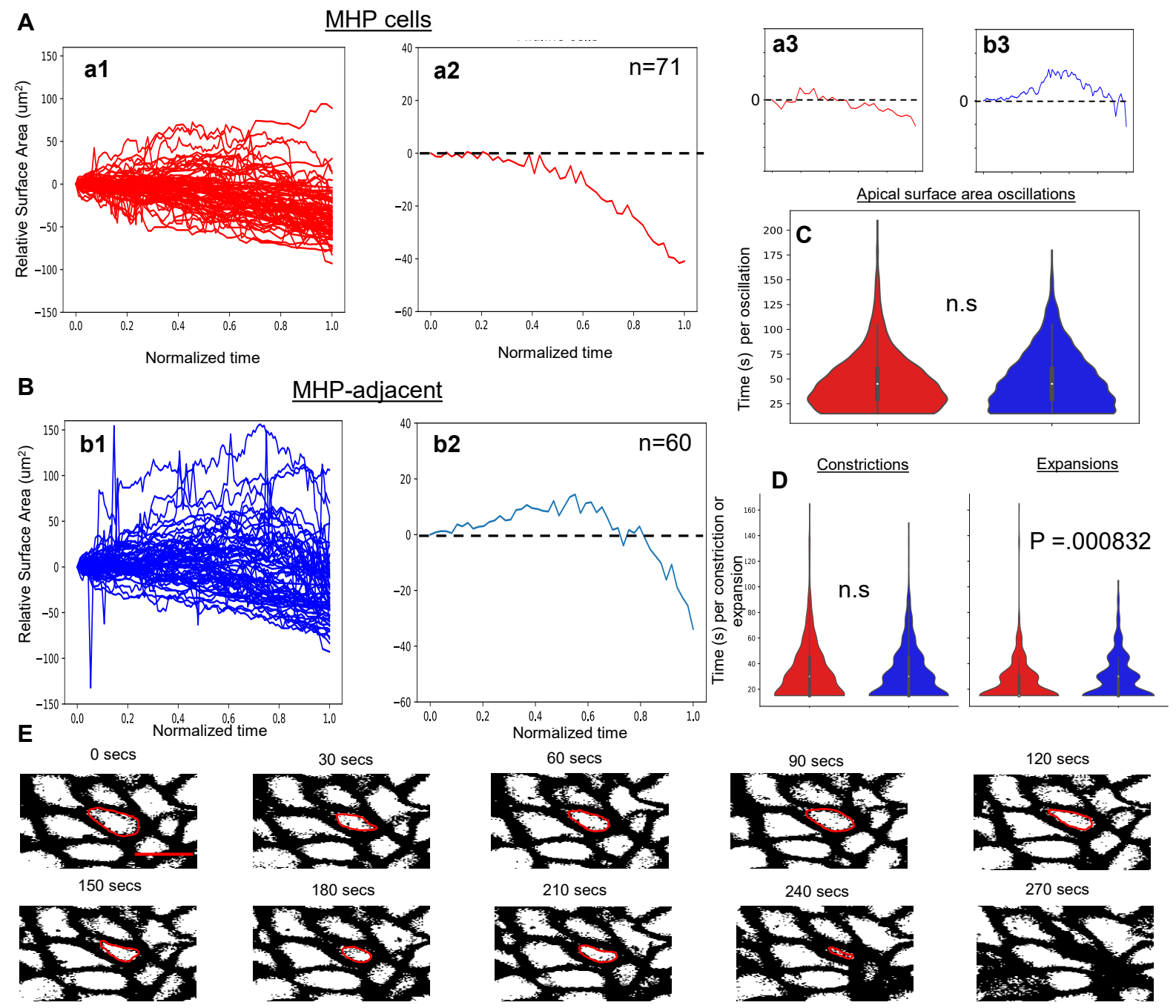
A
MHP cells
a1
Relative Surface Area (um²)
Normalized time
a2
n=71
Normalized time
a3
b3
Apical surface area oscillations
C
Time (s) per oscillation
n.s
B
MHP-adjacent
b1
Relative Surface Area (um²)
Normalized time
b2
n=60
Normalized time
Constrictions
Expansions
D
Time (s) per constriction or expansion
n.s
P =.000832
E
0 secs
30 secs
60 secs
90 secs
120 secs
150 secs
180 secs
210 secs
240 secs
270 secs

A

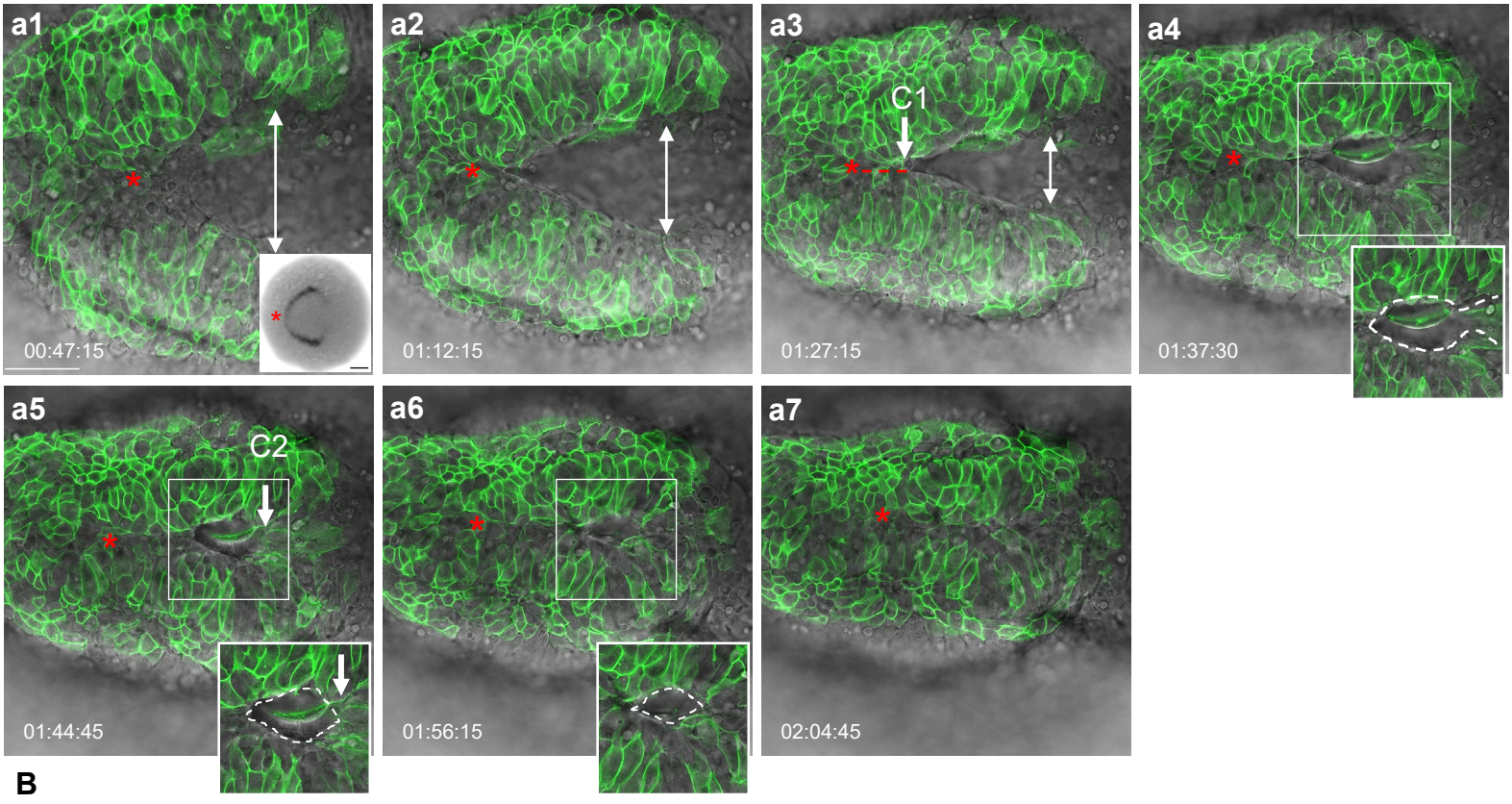
a1
00:47:15
a2
01:12:15
a3
C1
01:27:15
a4
01:37:30
a5
C2
01:44:45
a6
01:56:15
a7
02:04:45

B

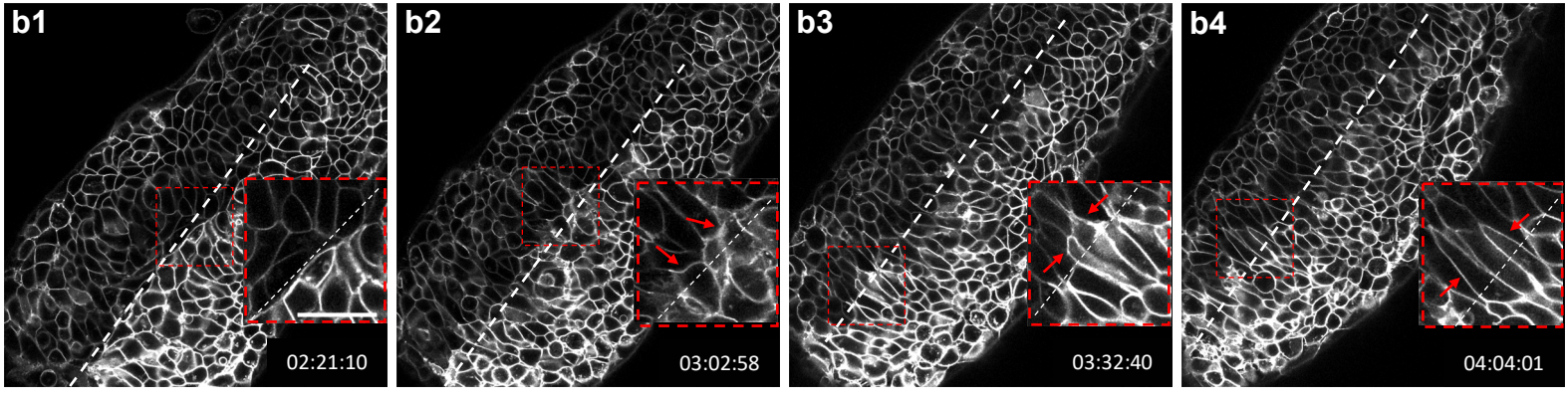
b1
02:21:10
b2
03:02:58
b3
03:32:40
b4
04:04:01

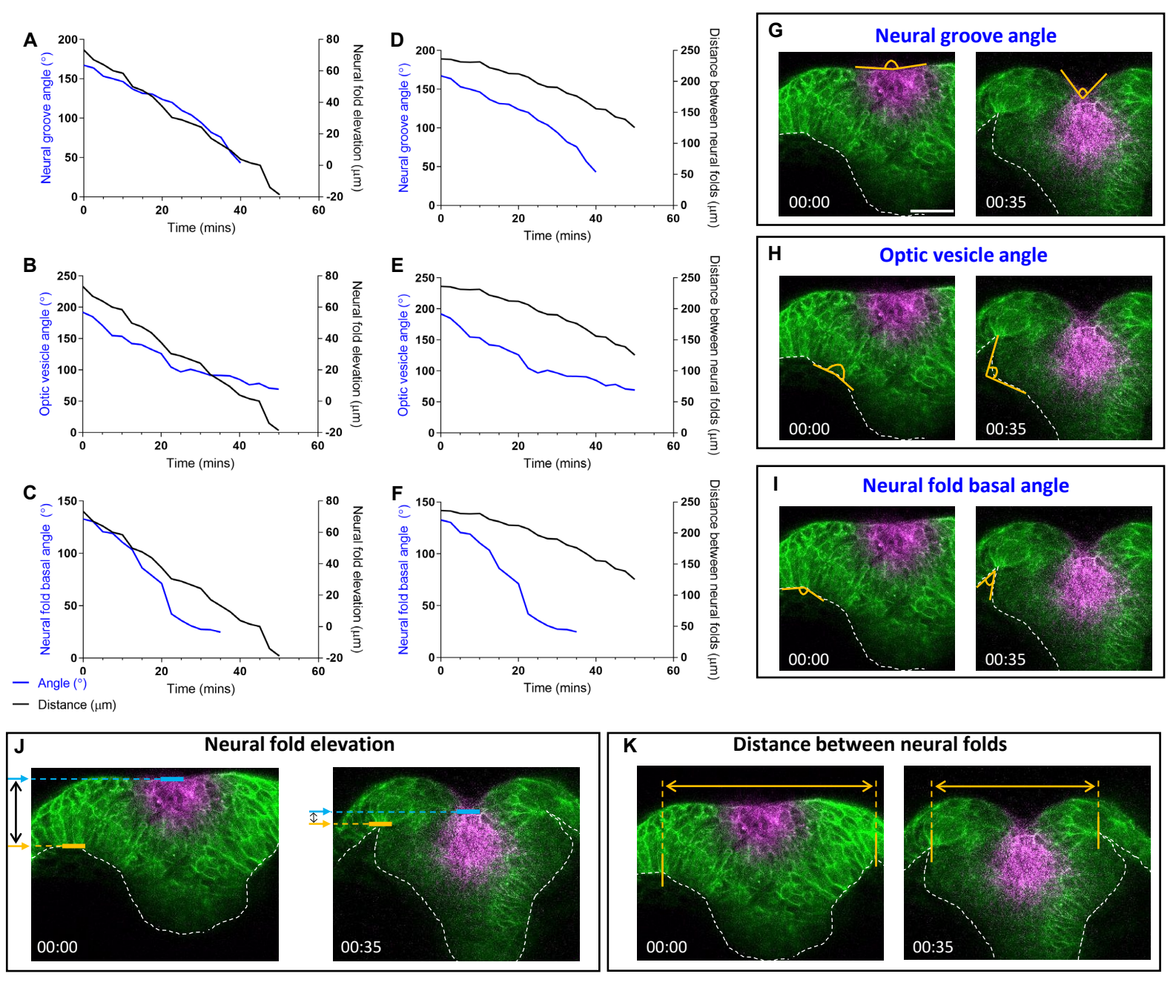
A
Neural groove angle (°)
Neural fold elevation (µm)
Time (mins)
B
Optic vesicle angle (°)
Neural fold elevation (µm)
Time (mins)
C
Neural fold basal angle (°)
Neural fold elevation (µm)
Time (mins)
Angle (°)
Distance (µm)
D
Neural groove angle (°)
Distance between neural folds (µm)
Time (mins)
E
Optic vesicle angle (°)
Distance between neural folds (µm)
Time (mins)
F
Neural fold basal angle (°)
Distance between neural folds (µm)
Time (mins)
G
Neural groove angle
00:00
00:35
H
Optic vesicle angle
00:00
00:35
I
Neural fold basal angle
00:00
00:35
J
Neural fold elevation
00:00
00:35
K
Distance between neural folds
00:00
00:35

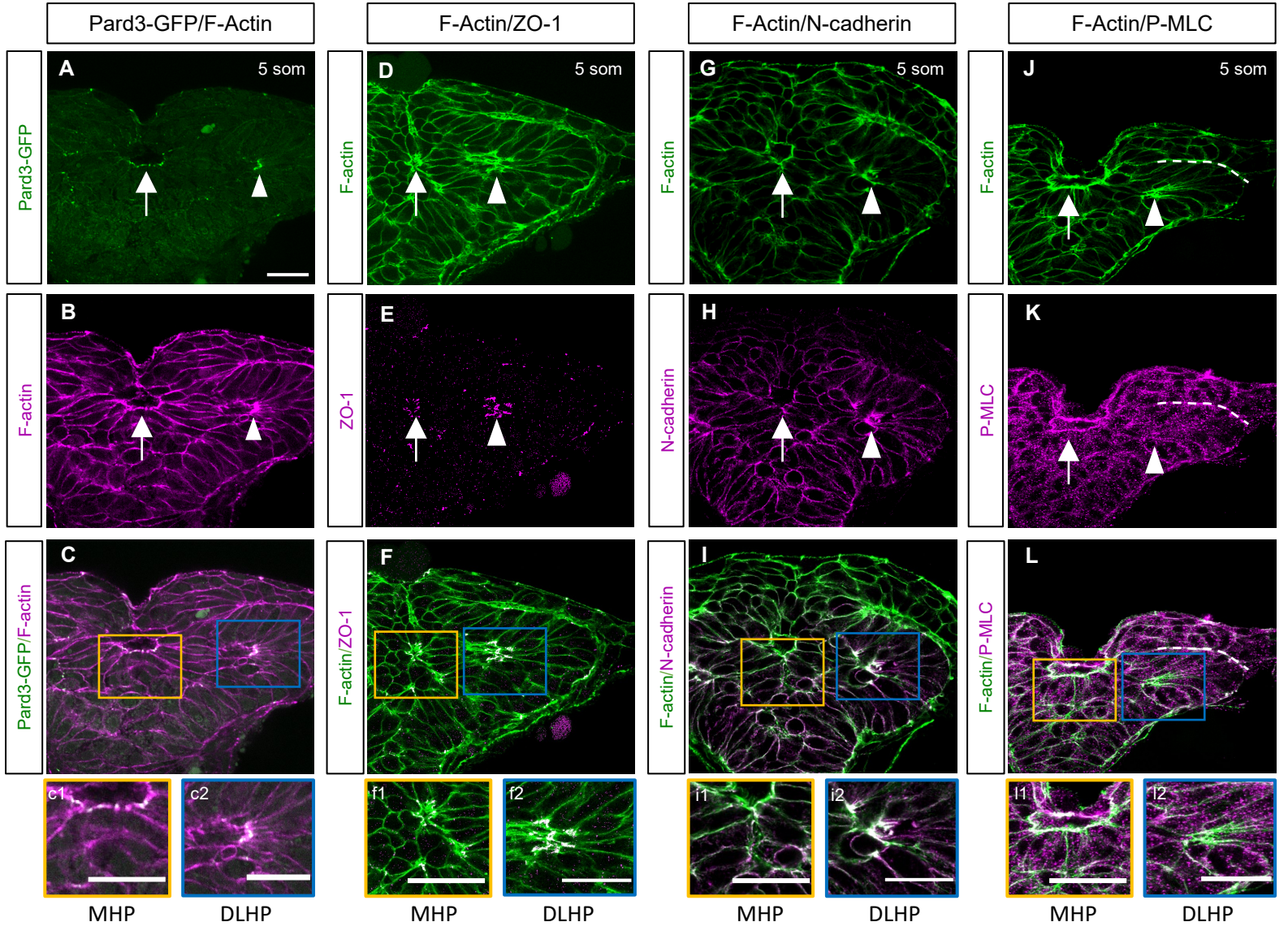
Pard3-GFP/F-Actin
F-Actin/ZO-1
F-Actin/N-cadherin
F-Actin/P-MLC
A
5 som
Pard3-GFP
B
F-actin
C
Pard3-GFP/F-actin
D
5 som
F-actin
E
ZO-1
F
F-actin/ZO-1
G
5 som
F-actin
H
N-cadherin
I
F-actin/N-cadherin
J
5 som
F-actin
K
P-MLC
L
F-actin/P-MLC
c1
c2
f1
f2
i1
i2
l1
l2
MHP
DLHP
MHP
DLHP
MHP
DLHP
MHP
DLHP

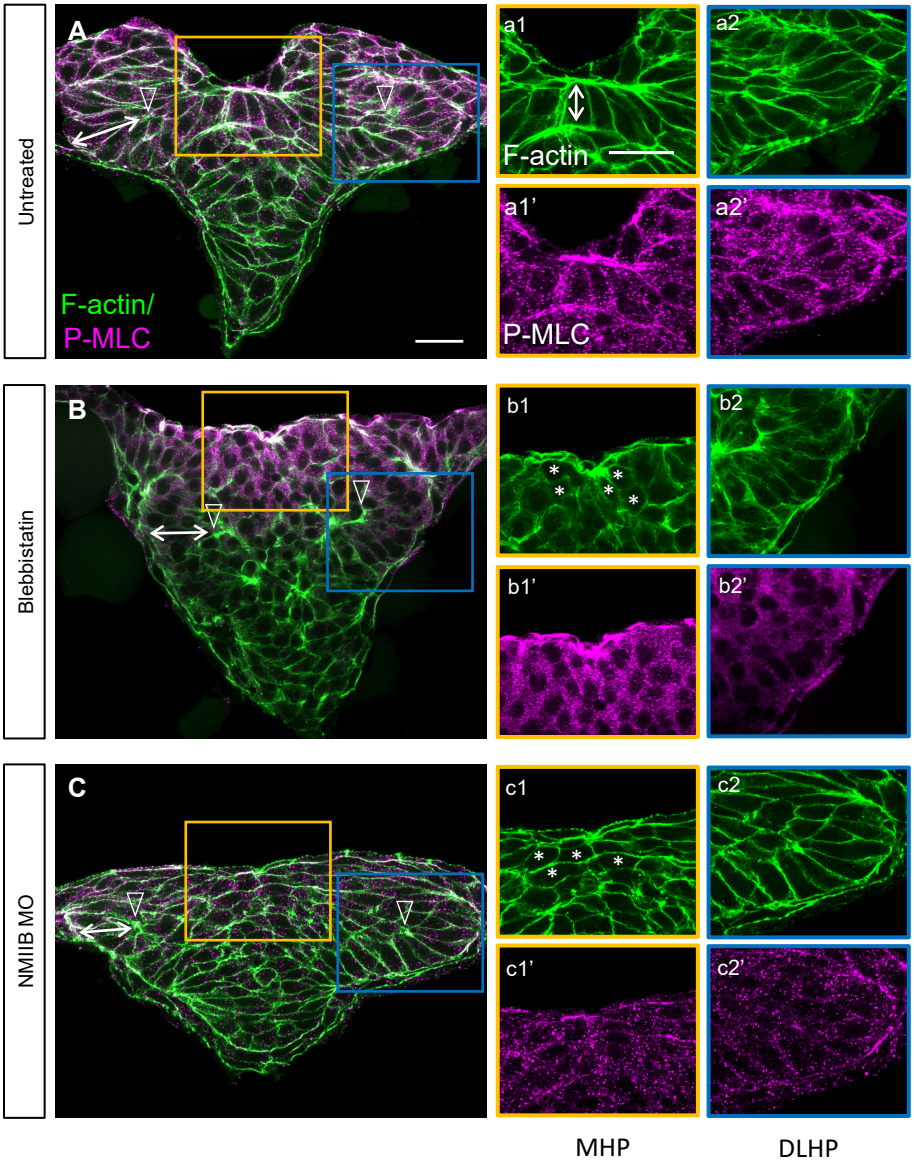
Untreated
Blebbistatin
NMIIB MO
A
B
C
F-actin/
P-MLC
a1
a2
a1'
a2'
F-actin
P-MLC
b1
b2
b1'
b2'
c1
c2
c1'
c2'
MHP
DLHP

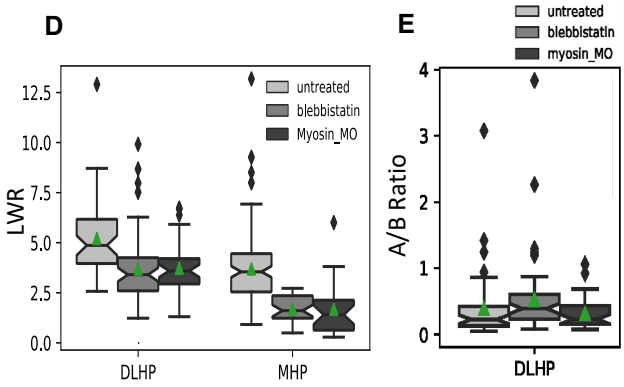
D
E
untreated
blebbistatin
Myosin_MO
LWR
12.5
10.0
7.5
5.0
2.5
0.0
DLHP
MHP
A/B Ratio
4
3
2
1
0
DLHP

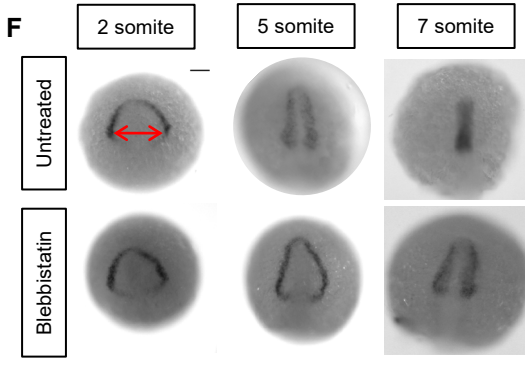
F
2 somite
5 somite
7 somite
Untreated
Blebbistatin

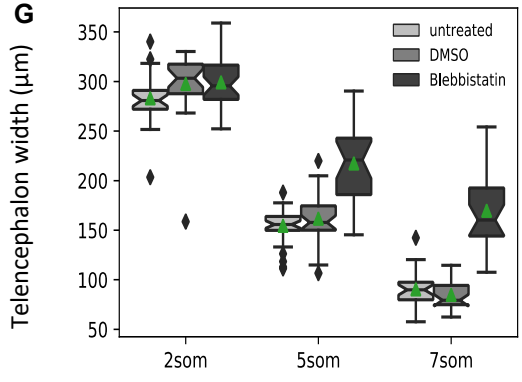
G
untreated
DMSO
Blebbistatin
Telencephalon width (µm)
350
300
250
200
150
100
50
2som
5som
7som